




# Silencing of amygdala circuits during sepsis prevents the development of anxiety-related behaviours

Lena Bourhy,<sup>1,2,3,†</sup> Aurélien Mazeraud,<sup>1,3,4,†</sup> Luis H. A. Costa,<sup>1,5</sup> Jarod Levy,<sup>2</sup> Damien Rei,<sup>2</sup> Estéban Hecquet,<sup>2</sup> Ilana Gabanyi,<sup>2,6</sup> Fernando A. Bozza,<sup>7,8</sup> Fabrice Chrétien,<sup>1,9</sup> Pierre-Marie Lledo,<sup>2,†</sup> Tarek Sharshar<sup>4,10,†</sup> and  Gabriel Lepousez<sup>2,†</sup>

<sup>†</sup>These authors contributed equally to this work.

See Desmedt (<https://doi.org/10.1093/brain/awac112>) for a scientific commentary on this article.

Sepsis is a life-threatening condition induced by a deregulated host response to severe infection. Post-sepsis syndrome includes long-term psychiatric disorders, such as persistent anxiety and post-traumatic stress disorder, whose neurobiological mechanisms remain unknown.

Using a reference mouse model of sepsis, we showed that mice that recovered from sepsis further developed anxiety-related behaviours associated with an exaggerated fear memory. In the brain, sepsis induced an acute pathological activation of a specific neuronal population of the central nucleus of the amygdala, which projects to the ventral bed nucleus of the stria terminalis. Using viral-genetic circuit tracing and *in vivo* calcium imaging, we observed that sepsis induced persistent changes in the connectivity matrix and in the responsiveness of these central amygdala neurons projecting to the ventral bed nucleus of the stria terminalis. The transient and targeted silencing of this subpopulation only during the acute phase of sepsis with a viral pharmacogenetic approach, or with the anti-epileptic and neuroprotective drug levetiracetam, prevented the subsequent development of anxiety-related behaviours.

Specific inhibition of brain anxiety and fear circuits during the sepsis acute phase constitutes a preventive approach to preclude the post-infection psychiatric outcomes.

- 1 Institut Pasteur, Université Paris Cité, Laboratory for Experimental Neuropathology, F-75015 Paris, France
- 2 Institut Pasteur, Université Paris Cité, CNRS UMR 3571, Perception and Memory Unit, F-75015 Paris, France
- 3 Université Paris Cité, Collège doctoral, F-75005 Paris, France
- 4 GHU Paris Psychiatrie Neurosciences, Service hospitalo-universitaire de Neuro-anesthésie réanimation, Paris, France
- 5 Department of Basic and Oral Biology, School of Dentistry of Ribeirão Preto, University of São Paulo, Ribeirão Preto, Brazil
- 6 Institut Pasteur, Université Paris Cité, Microenvironment and Immunity Unit, F-75015 Paris, France
- 7 National Institute of Infectious Disease Evandro Chagas (INI), OswaldoCruz Foundation (FIOCRUZ), Rio de Janeiro, Brazil
- 8 D'Or Institute for Research and Education (IDOR), Rio de Janeiro, Brazil
- 9 GHU Paris Psychiatrie Neurosciences, Service hospitalo-universitaire de Neuropathologie, Paris, France
- 10 Institut de Psychiatrie et Neurosciences de Paris (IPNP), INSERM UMR 1266, F-75014 Paris, France

Received March 29, 2021. Revised November 17, 2021. Accepted November 25, 2021. Advance access publication April 20, 2022

© The Author(s) 2022. Published by Oxford University Press on behalf of the Guarantors of Brain.

This is an Open Access article distributed under the terms of the Creative Commons Attribution-NonCommercial License (<https://creativecommons.org/licenses/by-nc/4.0/>), which permits non-commercial re-use, distribution, and reproduction in any medium, provided the original work is properly cited. For commercial re-use, please contact [journals.permissions@oup.com](mailto:journals.permissions@oup.com)

Correspondence to: Gabriel Lepousez  
 Laboratory for Perception and Memory Institut Pasteur  
 25 rue du Docteur Roux, 75724 Paris Cedex 15, France  
 E-mail: gabriel.lepousez@pasteur.fr

Correspondence may also be addressed to: Pierre-Marie Lledo  
 E-mail: pierre-marie.lledo@pasteur.fr

**Keywords:** neuroinflammation; neuro-immune interactions; cecal ligation and puncture; optogenetic; fear conditioning

**Abbreviations:** AAV = adeno-associated virus; AP = area postrema; BLA = basolateral amygdala; CeA = central nucleus of the amygdala; CLP = caecal ligation and puncture; CTB = cholera toxin B; LEV = levetiracetam; NTS = solitary tract nucleus; PBN = parabrachial nucleus; PKC $\delta$  = protein kinase C $\delta$ ; PTSD = post-traumatic stress disorder; vBNST = ventral bed nucleus of the stria terminalis

## Introduction

Sepsis is defined as a life-threatening organ dysfunction caused by a dysregulated host response to infection.<sup>1</sup> It is a medical emergency that, despite adequate early treatment, remains associated with a high mortality and increased long-term morbidities impacting the survivor's quality of life. It affects 30 million patients per year worldwide, with a growing incidence, making it an increasing burden in public health.<sup>2</sup> In 2017, considering its importance and complexity, the World Health Organization declared sepsis a global health priority, adopting a resolution to improve its prevention, detection and clinical management.<sup>3</sup>

Sepsis acute effects on the CNS induce behavioural and neuroendocrine adaptive response to systemic inflammation, referred to as sickness behaviour.<sup>4</sup> In addition to the sickness behaviour, 50–70% of patients develop a sepsis-associated encephalopathy, characterized by electroencephalographic alterations<sup>5</sup> and consciousness impairments—ranging from delirium to coma—which highly increases short-term morbi-mortality without being related to direct brain infection.<sup>6</sup> Interestingly, patients who clear the infection and survive sepsis develop later on severe psychiatric disorders including depression, anxiety and post-traumatic stress disorder (PTSD) that lead to increased suicide rates.<sup>5–12</sup> For instance, considering that lifetime PTSD prevalence is only 1–12% in the general population,<sup>7,8,13,14</sup> it reaches 24–50% in patients who recover from abdominal or respiratory sepsis. Despite the medical, epidemiological and social burden of these post-sepsis psychiatric disorders, there is to date no specific treatment to prevent or diminish their occurrence.

The pathophysiology and the mechanisms of the sepsis-associated encephalopathy are currently poorly understood. Some brain regions are preferentially targeted during sepsis. Studies of the brain of patients who died of sepsis demonstrate a strong neuronal activation and apoptosis in specific areas, notably the brainstem and the amygdala.<sup>9</sup> The amygdala, composed of two groups of nuclei—i.e. the basolateral region (BLA) and the central region (CeA)—is a crucial node in the fear and anxiety circuitry in both human and rodent studies.<sup>15,16</sup> The CeA, and more specifically its lateral subdivision (CeL), contains mainly GABAergic neurons that project to the centres controlling defensive and appetitive behaviour.<sup>17</sup> These CeA output neurons are composed of two non-overlapping subpopulations of inhibitory neurons, which express the markers protein kinase C $\delta$  (PKC $\delta$ ) or somatostatin (SOM<sup>+</sup>) that reciprocally control each other, leading to the expression of conditioned fear, notably in fear learning, extinction and generalization.<sup>15,17</sup> Importantly, PKC $\delta$  neurons receive direct inputs from the parabrachial nucleus (PBN), a brainstem

structure which provides nociceptive and vagal signals.<sup>18</sup> Moreover, inhibition of PKC $\delta$  neurons is sufficient to drive the formation of artificial aversive memories,<sup>19</sup> indicating the crucial role of PKC $\delta$  neurons in the fear memory network.<sup>20</sup> In addition, optogenetic activation of PKC $\delta$  neurons in the CeL promotes anxiogenic<sup>21</sup> and anorexic effects,<sup>22</sup> suggesting a diversity of subcircuits within the overall PKC $\delta$  neuron population. From the acute adaptive defensive behaviour controlled by the CeA can emerge a delayed sustained maladaptive response. This response is characterized by an overestimation of the threat potential in uncertain situations and involves an overlapping circuit centred on the amygdala, whose dysfunction has been highlighted in various psychiatric disorders.<sup>23</sup> Additionally, the extended amygdala—which includes the CeA and the bed nucleus of the stria terminalis (BNST)—has been shown to play a predominant role in the outcome of anxiety-related disorders including PTSD.<sup>24,25</sup>

Using the common murine sepsis model of caecal ligation and puncture (CLP) that induces sepsis by an intra-abdominal infection, it is possible to experimentally reproduce the sepsis-induced brain responses described herein.<sup>26</sup> It mimics the major features of human sepsis, including strong inflammatory response and sickness behaviour.<sup>27–29</sup> Studies have shown that mice present anxiety-like behaviour and altered fear memory several weeks after CLP induction, reminiscent of the anxiety and PTSD-like symptoms developed by human sepsis survivors.<sup>30–34</sup> In the present study, this preclinical model has been used to study the causal link between the sepsis-induced brain dysfunction during the acute phase and the subsequent development of PTSD-like fear expression. We demonstrated that sepsis induced an acute and transient pathological activation of a specific circuit of the extended amygdala. The inhibition of this neuronal subpopulation only during the acute phase of sepsis prevented the development of post-sepsis PTSD-like symptoms. From a therapeutic perspective, it is noteworthy that, in addition to this transient neuronal hyperactivation, sepsis-associated encephalopathy has been characterized by EEG changes,<sup>5,35</sup> including a shift of alpha and beta activities to increased delta and theta activities, with triphasic waves and burst suppression in the most severe cases. Epileptic discharges are detected in more than 10% of patients with sepsis-associated encephalopathy.<sup>36</sup> In rodent studies, the injection of the bacterial endotoxin liposaccharide increases seizure susceptibility by lowering seizure threshold.<sup>37</sup> Given these observations, we tested the effect of the administration during sepsis of levetiracetam (LEV), an anti-epileptic and neuromodulatory drug. LEV is a presynaptic

inhibitor of the neurotransmitter release and the most frequently used anti-epileptic drug, very well tolerated even in critically ill patients.<sup>38</sup> LEV acts on the synaptic vesicle glycoprotein 2A located at the surface of the neurotransmitter vesicle in the presynaptic terminal and inhibits vesicle release in the synaptic cleft.<sup>39</sup> LEV has a pan-synaptic activity specifically on bursts of activity and is non-sedative. Moreover, studies demonstrated its capacity to restore alpha and beta activities with reducing the delta and theta ones in epileptic patients.<sup>40</sup> Besides its classical anti-epileptic action, LEV has been used to dampen pathological hyperexcitability of neocortical circuits in neurodegenerative diseases<sup>41</sup> and in ischaemic brain injuries.<sup>42</sup> In the present study, we administered LEV during the acute phase of sepsis to investigate whether LEV could significantly prevent the CLP-induced transient neuronal activation of amygdala circuits and reduced the magnitude of post-sepsis anxiety and PTSD-like fear expression.

## Materials and methods

### Animals

Adult (2–5 months old) wild-type male C57Bl/6J mice (Janvier Labs) and adult male and female FOS-CreERT2 (Fos<sup>tm1.1(cre)/ERT2</sup>Luo, Jackson Labs<sup>43</sup>) and VGAT-ires-Cre mice (Slc32a1<sup>tm2(cre)Low1</sup>, Jackson Labs<sup>44</sup>) were housed under a 12-h light/dark cycle, with dry food and water available *ad libitum*. All procedures were consistent with the European Union guidelines (EU Directive 2010/63/EU) for animal experiments and were reviewed and approved by the Animal Welfare Committee of the Institut Pasteur (Project numbers: 2015-004, 2013-0086, dap180018 and dap200025).

### Caecal ligation and puncture surgery

Mice were treated for analgesia and rehydration 30 mins before surgery with subcutaneous (s.c.) injection of buprenorphine (0.1 mg/kg, Buprecare®, Axience) and saline (NaCl 0.9%). The CLP surgery (~10 min) was achieved under general anaesthesia (isoflurane, 4% for induction in inhalation chamber, then maintained during the surgery at 1.5% with 98.5% oxygen). Mice were placed on a heating pad to maintain the body temperature at 37°C during the procedure. Absence of reaction to leg and tail pinch was checked before incision of the abdominal wall previously cleaned with ethanol 70%, and then incision of the peritoneum. The caecum was exposed and a loose ligation was achieved at its external third with Mersilk 4.0 (Ethicon). Two transfixing punctures were performed avoiding blood vessels with a 21G needle. Faeces were expressed and spread on the caecum before suturing abdominal muscles and peritoneum in two separate plans. Buprenorphine and saline subcutaneous injections were then performed every 12 h until complete recovery. We evaluated sepsis severity every 12 h for 72 h using the sepsis score, which evaluates the clinical signs of local (abdominal spasm) and systemic reaction to sepsis (rectal temperature, fur erection, abnormal breathing), behavioural changes (faeces cleaning, presence of peri-ocular dried eye drop, incomplete palpebral opening, spontaneous activity in the cage, escape attempt after tail grabbing) and muscular weakness (ability to grip forceps, body tone, difficulty walking). Each item of the scale was scored 0 or 1, with a total score range from 0 (normal) to 12 (highly severe). For ethical reasons, mice with a sepsis score  $\geq 6$  and a temperature  $\leq 35.3^\circ\text{C}$  were euthanized. CLP mice were compared either to sham animals, which only underwent a laparotomy procedure with the same anaesthetic and analgesic protocol as CLP mice, or to control-naïve animals that only underwent the same

anaesthetic and analgesic protocol as CLP mice. CLP, sham and control surgery were performed in the morning (Zeitgeber time 3–5). Significant variability in the sepsis score was observed using such a CLP protocol. Variability factors include the surgical procedure itself, but also the microbiota and the digestion state of the animals at the time of the surgery. To avoid this variability as much as possible, CLP surgeries were carried out by the same experimenters following the similar protocols at the same period of the day and in the same animal facility. Compared to previous works, the mean features of our CLP protocol are that it is performed on a heating pad under isoflurane anaesthesia (which allows a very rapid awakening of the animal) and under analgesia with buprenorphine without any other post-surgical treatment such as antibiotics. Mice were kept warm by the heating pad and regularly injected with buprenorphine and saline during the 72 h following surgery. The final lethality of the CLP protocol was ~50% (Supplementary Fig. 1A and B).

### Stereotaxic injections

Mice were transported to the room where the surgery was performed and underwent a subcutaneous injection of buprenorphine (0.1 mg/kg, Buprecare, Axience) and saline (NaCl 0.9%) 30 min before anaesthesia. Mice were anaesthetized with an intraperitoneal (i.p.) injection of xylazine (10 mg/kg, Rompun 2%, Bayer) and ketamine (50 mg/kg, Imalgene, Merial) and then placed on a heating pad to maintain body temperature at 37°C. Stereotaxic injections of viral vectors in adult mice were performed as previously described.<sup>45</sup> Briefly, the animal's head was inserted into a stereotaxic frame (David Kopf Instruments). Following local anaesthesia (lidocaine, Xylovet), the animal's head was shaved, the scalp sterilized with an iodine solution and cut to reveal the skull. Small craniotomies were drilled and the tip of the pulled glass pipettes (tip diameter, ~30–50  $\mu\text{m}$ ) of the injection system (Nanoinject II, Drummond) were slowly lowered to the target coordinates. AAV9-hSyn-FLEX-ChrimsonR-TdTomato-WPRE (Penn vector core,  $4.5 \times 10^{12}$  vg/ml, 100 nl injected bilaterally, speed: 1 nl/s), AAV9-hSyn-FLEX-GFP-2A-Synaptophysin-mRuby-WPRE (Addgene plasmid 71760; production by the Translational Vector Core of the laboratory for Translational Research in Gene Therapy, INSERM UMR1089, Université de Nantes, France  $5 \times 10^{12}$  vg/ml, 100 nl injected bilaterally), AAV9-Syn-FLEX-GCamp6F.WPRE.SV40 (Addgene 100833,  $3 \times 10^{13}$  vg/ml, 50 nl injected bilaterally), AAV5-hSyn-DIO-mCherry-WPRE (Addgene 50459,  $2.5 \times 10^{13}$  vg/ml, diluted 1:5 in saline 0.9%, 50 nl injected bilaterally), AAV5-hSyn-DIO-hM4D-mCherry (Addgene 44362,  $4.5 \times 10^{12}$  vg/ml, 50 nl injected bilaterally), AAV5-hSyn-DIO-hM3D-mCherry (Addgene 44361,  $5 \times 10^{12}$  vg/ml, 50 nl injected bilaterally), pAAV-synP-FLEX-splitTVA-EGFP-B19G (Addgene 52473,  $10^{13}$  vg/ml, 50 nl injected bilaterally) or (EnvA)SAD- $\Delta$ G-mCherry (provided by Karl-Klaus Conzelmann,  $10^9$  vg/ $\mu\text{l}$ , 50 nl injected bilaterally) were injected in the CeA (from bregma, antero-posterior: -1.25, medial lateral:  $\pm 2.85$ , dorsoventral from brain surface: -4.0). AAVretro-EF1a-mCherry-IRES-Cre (Addgene 55632,  $1.4 \times 10^{12}$  vg/ml, 100 nl injected bilaterally), AAVretro-PGK-Cre (Addgene 24593,  $2 \times 10^{13}$  vg/ml, 100 nl injected bilaterally), AAV9-hSyn-GCaMP6f-WPRE (Addgene 100837,  $2 \times 10^{13}$  vg/ml, 100 nl injected bilaterally) or cholera toxin B (CTB) A647 (Invitrogen C34778, 1 mg/ml, 300 nl injected bilaterally) was injected in the ventral BNST (vBNST) (antero-posterior: +0.2, medial lateral:  $\pm 1.0$ , dorsoventral: -4.2). Injection in the vBNST encompassed the lateral and medial part of the vBNST below the anterior commissure,<sup>46</sup> with the commissure limiting the diffusion of the virus to dorsal regions of BNST.

CTB A568 (Invitrogen C34777, 1 mg/ml, 300 nl injected bilaterally) was injected in the substantia innominata (antero-posterior:  $-0.3$ , medial lateral:  $\pm 1.9$ , dorsoventral:  $-5.0$  from brain surface). At the end of the injection, the skin was sutured and then sterilized with iodine solution. The animal was left to recover and then transferred back to its home cage. Animals in which *post hoc* histological examination showed that viral injections were not in the correct location were excluded from analysis.

### EEG and amygdala local field potential recordings

Following analgesia (buprenorphine, 0.1 mg/kg s.c.) and anaesthesia (ketamine and xylazine, 50 and 10 mg/kg, respectively, i.p.), mice were placed into a stereotaxic frame (David Kopf Instruments). Following craniotomy, two EEG silver-wire electrodes (250  $\mu$ m silver wire with a 1-mm ball tip head, A-M Systems Inc.) were implanted epidurally above the dorsal hippocampus (from bregma, anteroposterior:  $-2$  mm, medial lateral:  $-1.5$  mm), two reference electrodes implanted on the occipital crest (250- $\mu$ m silver wire with a 1-mm ball tip head) and two EMG wires inserted between the neck muscles (280- $\mu$ m insulated silver wire), the six electrodes having been previously soldered to a miniature eight-pin connector (Omnetics). For local field potential (LFP) recordings in the amygdala, a bipolar electrode (twisted 50- $\mu$ m coated-platinum wires, impedance 0.2–0.5 M $\Omega$ , A-M Systems Inc.) was lowered into the left amygdala, with the tip of the bipolar electrode positioned into the CeA (from bregma, anteroposterior  $-1.25$ , medial lateral  $\pm 2.9$ , dorsoventral  $-4.15$ ). The whole system was stabilized with a liquid bonding resin (Superbond, Sun Medical) and dental acrylic (Unifast). The animals were left in their individual cage to recover for 2 weeks. Mice were then habituated to the connection/disconnection of a flexible connection cable for several days and then continuously recorded within their individual cage for three to five consecutive days. Following this baseline recording, animals were disconnected, experienced just a general anaesthesia/analgesia ( $\sim 10$  min isoflurane anaesthesia at Zeitgeber time 4–5 and buprenorphine, 0.1 mg/kg s.c.) and were then immediately reconnected to the cable for a 24-h recording. The day after, following a baseline recording, mice underwent a CLP surgery under anaesthesia/analgesia ( $\sim 10$  min surgery performed at Zeitgeber time 4–5 and buprenorphine, 0.1 mg/kg s.c.) and were then immediately reconnected to the cable. EEG, EMG and LFP signals were amplified ( $\times 1000$ , 0.1–300 Hz, IsoDAM8A, World Precision Instruments) and sampled (Micro1401-3 A/D interface, CED) at 1 kHz. The signals were filtered by a digital finite impulse response (FIR) filter (EEG: 0.1–30 Hz; EMG: 10–300 Hz; LFP: 1–300 Hz). For EEG/EMG, we extracted the EEG power spectrum for non-overlapping 3-h epochs before and after the treatment. We computed the total power (0.1–100 Hz), the ratio between the delta band (1–5 Hz) power and the theta band (6–10 Hz) power (delta/theta ratio), and the mean frequency in the theta-delta band (0.1–10 Hz). Given the massive EEG alterations in both power and frequency after CLP, classical sleep scoring algorithms could not be used properly. As an alternative to evaluate total sleep time and sleep bout duration during the 6 h post-CLP (compared to control recordings after just anaesthesia/analgesia), we analysed the EMG signal to extract all the time bouts the animals spent immobile for more than 20 s, and then calculated the mean resting bout duration, the cumulative time the animal spent at rest and the cumulative time the animals spent in prolonged rest (more than 120 s). For LFP *post hoc* analysis and epileptiform-like spike extraction, we applied spike detection (time window,  $-100$  ms;  $+300$  ms), spike sorting, spike clustering function and spike waveform analysis using Spike2

software (CED) followed by a manual adjustment of the clusters. Using this analysis, we could extract stereotyped epileptiform spikes—characterized by a fast and sharp spike ( $\sim 50$  ms; 50–100  $\mu$ V) followed by a slow wave-like component, which clearly distinguished from the background activity—and excluded most electrical/movement artefactual events. Investigators were not blinded to the group identity, but automatic analysis routines were performed with the same script executed for each experimental group.

### Tamoxifen-inducible recombination

Three hours after CLP, we injected 4-hydroxy-tamoxifen [1 mg/kg diluted in saline with 2.5% dimethyl sulphoxide (DMSO), 2.5% Kolliphor]. Half the amount of tamoxifen was administered subcutaneously, the other half intraperitoneally. The control mice were injected with a vehicle solution without 4-hydroxy-tamoxifen (saline with 2.5% DMSO, 2.5% Kolliphor).

### In vivo calcium imaging with fibre photometry

Following the injection of the GCaMP6f-expressing viral vector, optic fibres (multimode,  $\varnothing$  430  $\mu$ m, NA 0.5, LC zirconia ferrule) were implanted bilaterally at the same injection coordinates and fixed to the skull with a liquid bonding resin (Superbond, Sun Medical) and dental acrylic (Unifast). Three weeks after implantation, neurons infected with GCaMP6f vector were chronically excited with a 473-nm solid-state laser (Crystal Lasers) via a 430- $\mu$ m multimode optical fibre (output intensity  $< 0.1$  mW). The emitted fluorescence was collected by the same fibre, filtered through a dichroic mirror and a GFP-emission filter (452–490 nm/505–800 nm; MDF-GFP, Thorlabs), filtered ( $525 \pm 19$  nm) and then focused on a NewFocus 2151 Femtowatt photodetector (Newport). Blue light reflected in the light path was also filtered and measured with a second amplifying photodetector (PDA36A; Thorlabs). The signals from the two photodetectors were digitized by a digital-to-analogue converter (Micro1401-3 A/D interface, CED) at 5000 Hz and then recorded using Spike2 software (CED, UK). For light-stimulation of ChRimsonR-expressing axon terminals coupled in GCaMP6f recordings, red light (589 nm, 10 mW, pulse duration: 15 ms) was collimated in the recording optic fibre to selectively activate ChRimsonR-expressing axon terminals while GCaMP6f was independently excited with low blue light intensity ( $< 0.1$  mW), thereby avoiding cross-excitation of ChRimsonR. Mice were progressively habituated to the bilateral connection of two flexible optical patchcord cables (Doric Lenses Inc.) within their individual home cage. Recordings were made *in situ* in the home cage 4 h before and up to 24 h after surgery (CLP or sham). For each animal, we also performed a control recording before and after general anaesthesia without surgery (10 min of isoflurane 4% induction followed by 10 min maintained at 1–1.5% with 98.5% oxygen). Recordings with low-fluorescence signals (mean fluorescence  $< 0.2$  mV and/or spontaneous events in  $\Delta F/F < 1\%$ ) or displaying movement/laser artefacts (visible in the reflected blue light channel) were discarded from the analysis. For analysis of fluorescence signals, the raw GCaMP6f signal traces from each detector were first smoothed (smoothing window = 0.02 s) and then used to calculate a continuous  $\Delta F/F$ , defined as  $[F(t) - F_0(t)] / F_0(t)$ , where  $F(t)$  is the raw-smoothed GCaMP6f signal trace and  $F_0(t)$  is the mean fluorescence intensity within sliding window (10 s) centred on time  $t$ . To extract spontaneous calcium transient with the same threshold in all individuals independently of their  $\Delta F/F$  amplitude, we also calculated a z-score-normalized fluorescence  $F'$ , defined as

$[F(t) - F_0(t)] / \sigma(t)$ , where  $\sigma(t)$  is the standard deviation of the  $F(t)$  signal in a sliding window (100 s) centred on time  $t$ . From this z-score-normalized fluorescence  $F'$ , all the events above 3SD were automatically extracted with custom scripts (Spike2, CED; minimum time interval between events, 2 s) and the peak amplitude of each event was then extracted from the  $\Delta F/F$  signal. The frequency of the sorted spontaneous events was then reported as the number of events per unit of time (30 min) and normalized to the 2-h baseline activity before treatment (baseline set to 1). For the mean fluorescence analysis, the row GCaMP6f signal traces were downsampled (0.5 Hz), smoothed (100 s), averaged every 30 min and normalized to the 2-h baseline mean fluorescence before treatment. Investigators were not blinded to the group identity, but automatic analysis routines were performed with the same script executed for each experimental group. Animals in which post hoc histological examination showed that viral injection or implanted optic fibre were mislocated were excluded from further analysis.

### Pharmacology

Clozapine-N-oxide (CNO) (C0832; Sigma-Aldrich, resuspended in 0.9% NaCl saline, 1 mg/kg) was injected intraperitoneally at time 0 hours (H0), H6, H12, H24, H30, H36 and H48, according to the experiment. Levetiracetam (Union Chimique Belge, resuspended in 0.9% NaCl saline, 300 mg/kg) was injected intraperitoneally at H0, H12, H24, H36 and H48 post-CLP.

### Intracerebroventricular continuous infusion of levetiracetam

Twenty-four hours before surgery, Alzet osmotic pumps (model 1003D, 1  $\mu$ l/h for 3 days) coupled to brain infusion kit (model #3) were filled with LEV (or sterile saline as control), and then activated by immersing the pumps into sterile saline and incubating it in a 37°C incubator to allow a partial 1 day pumping (out of the 3 days). For surgery, mice were shaved, locally sterilized and placed into a stereotaxic frame (David Kopf Instruments) under analgesia (buprenorphine, 0.1 mg/kg s.c.), local anaesthesia (lidocaine) and general anaesthesia (isoflurane, 4% for induction in inhalation chamber, then maintained during the surgery at 1.5% with 98.5% oxygen). Following craniotomy, osmotic pumps were inserted into a subcutaneous tunnel between the two scapulae and the brain infusion cannula was implanted into the right lateral ventricle (stereotaxic coordinates relative to bregma, antero-posterior: -0.5 mm; medial lateral: 1 mm; dorsoventral: 2.5 mm). Immediately after osmotic pump implantation and the suture of the skin, CLP was performed as described above. LEV concentration for intracerebroventricular (ICV) infusion (100 mg/ml; 0.1 mg/ $\mu$ l/h) was calculated based on previous studies using ICV LEV administration (0.3 mg/h<sup>47</sup>) and also calculated based on studies that have established the ED<sub>50</sub> for anticonvulsant effects of the anti-epileptic drug valproate with intraperitoneal and ICV injection mode, indicating that a dilution factor of ~8–18 between intraperitoneal and ICV mode have an equivalent seizure suppression performance.<sup>48</sup>

### Behavioural experiments

Behavioural assays started 15 days after CLP. For each experiment, mice were transported in their home cage to the experiment room 45 min prior to experiments. A 100-lx light was used, and mice were tracked with a JVC lowlux camera fixed to the ceiling above the arenas. The same experimenter blinded to the experimental treatment analysed the videos with Ethovision XT (Noldus).

### Open field test

Open field arenas were composed of four opaque 50 × 50 × 50 cm squared cages without bedding, disposed in a 2 × 2 rectangle. Spatial cues consisted in three vertical lines or a triangle of green labelling tape on opposing north and south walls. Mice were released in the centre facing a given wall and were allowed to move freely and explore the cage for 15 min. Total distance moved (cm), mean distance to centre (cm) and time spent moving (s) were computed from tracked videos with Ethovision XT software.

### Novel object location/novel object recognition

Novel object localization and novel object recognition arenas were the same arenas as used in the openfield. Animals were habituated to the behavioural arena for 3 days (15 min on the first day and then 10 min per day on the next 2 days) before beginning the object training. On the third day, after the last habituation period, the training phase of the novel object localization protocol was started. Two identical objects (either two 50-ml falcon tube caps or two four-plot yellow Lego Duplo bricks) were placed on one side of each arena. At the beginning of the trial, the mouse was placed facing the middle of the wall opposite the objects. During two 10-min training sessions, mice became familiarized with the objects—sessions being separated by an inter-trial interval of 1 h. One hour after the last habituation phase, the novel location task trial was started after moving one object to the opposite corner. Mice were placed into the arenas for a further 10 min. The training phase for the novel object recognition began immediately after the novel object localization trial. Mice freely explored the arenas for a further 10 min after the two objects were placed in their original location. Twenty-four hours, one of the objects was substituted with a different one (for instance, one of the two 50-ml falcon tube caps by a four-plot yellow Lego Duplo brick and vice versa). For both tests, the time spent with each object (old and new locations or old and new objects) was recorded during a 5-min test period. Mice were considered exploring when obvious signs of directed attention were observed (i.e. sniffing or prolonged observation). Time spent on top of the objects was not counted, unless the mice showed simultaneously a direct attention to the object. For novel object localization and novel object recognition experiments, the discrimination index was calculated by dividing the time (in seconds) spent exploring a new object (or new location) by the sum of the time (in seconds) exploring the familiar and new objects (or location).

### Light/dark box test

The light/dark box arena consisted of two equal-sized arenas: a white and opened one and a black and covered one, communicating through a mouse-sized open door. Mice were placed at the beginning of the test in the light arena and were recorded during a 6-min trial. The percentage of time spent in the light arena was calculated with the Ethovision XT software.

### Olfactory habituation

Mice were habituated to a transparent cage with perforated aluminium soil without bedding (46 × 24 × 20 cm) for 20 mins before the test. A paper filter soaked with 10  $\mu$ l of amyl acetate (1% in mineral oil, Sigma-Aldrich) was presented lying on a Parafilm® sheet for 2 min, three times, with an inter-trial interval of 2 min. Mice were considered sniffing when their nose was directly above the filter paper. On the fourth trial, a new odour (10  $\mu$ l of eugenol, 1% in mineral oil, Sigma Aldrich) was presented for 3 min. The sniffing

times between the fourth and the third trials were then compared. For each mouse, each investigation time was normalized to investigation time during the first odour presentation.

### Morris water maze

A Morris water maze task was performed in a 120-cm water tank filled with opacified water (white paint, Crayola) maintained at  $21 \pm 1^\circ\text{C}$  during the experiment. Spatial cues (triangle, circle, rectangle, cross) were disposed at each cardinal point. A circular platform (11 cm) was placed in the south-west quadrant 2 cm above the water level for the first two trials of the first day and then 2 cm below the water surface for all remaining trials. The test encompassed a training period and a probe trial. The training period consisted of four trials per day until the learning was considered satisfactory (see below). To avoid track memorization, mice were released in the water tank at a different position from one trial to the next, always facing the closest wall. The trial was stopped when the mouse found the platform and, if not, systematically after 60 s from the release. Mice were allowed to stay 10 s on the platform before placing them back in their home cage. When mice failed to find the platform, they were placed on it for 10 s. For each trial, the latency before reaching the platform (s), path length (cm) and time spent in each quadrant (s) were computed. When latency before reaching the platform was  $<20$  s, learning was considered completed and the probe trial test was then achieved 24 h later. During the probe trial, the platform was removed and mice were released in the quadrant opposite to the previous site of the platform. Time spent in the quadrant where the platform was placed was then calculated. Ethovision XT and MUST-C algorithm were used to analyse individual mice track and strategy to reach the platform site. MUST-C provides an unbiased classification and scoring of the strategy used to find the platform from highly cognitive to non-cognitive strategies (6/6 = direct, 5/6 = corrected, 4/6 = focused search, 3/6 = circling, 3/6 = accidental circling, 3/6 = chaining, 2/6 = random, 1/6 = thigmotaxis and 1/6 = passivity).<sup>49</sup>

### Auditory and contextual fear conditioning

For the fear conditioning, mice were individually placed in a home-made electrifiable grid floor Plexiglas arena ( $20 \times 15$  cm) contained in a sound-proof box connected to a constant-current (DC) shock generator (Supertech Instruments) and equipped with a camera and an audio speaker. Before each conditioning session, the cage was washed with Surfa'Safe® premium (Anios). After a 3-min habituation period, mice underwent two sequences of a 28-s 2.5-kHz tone (conditional stimulus, repetition frequency: 440 Hz, 75 dB) followed by a 2-s electric shock (0.4 mA, unconditional stimulus) separated by a 15-s silence period, then followed by a 1-min resting period. Movement following shock was monitored through a camera placed above the arena. Fear recall was performed 24 h after conditioning. The conditioning and the contextual recall environment were identical. Mice behaviour was recorded for 3 min. Immediately after the contextual exposure trial, the auditory exposure trial was started. Mice were moved to a different  $20 \times 20$  cm cage, with a smooth floor (Plexiglas) and different olfactory cue (as the cage was washed with ethanol 75% and odorized with amyl acetate 1%). After a 2-min habituation time, mice were exposed for 2 min to the 2.5-kHz unconditional auditory stimulus (repetition frequency: 440 Hz, 75 dB). For the contextual and the auditory fear recalls, live freezing time was evaluated. Freezing was defined as the absence of movement except for breathing. A blind second evaluation of the freezing time was achieved based

on the videos recorded during the sessions. Animals not showing proper active avoidance during the two consecutive foot shocks were discarded from the analysis ( $<5\%$  of animals).

### Fear extinction

For auditory fear extinction, mice were exposed immediately after auditory recall to a series of 1030-s conditional auditory stimuli (2.5 kHz, repetition frequency: 440 Hz, 75 dB), separated by an inter-trial period of 15 s in the same cage context as the auditory fear recall. Auditory fear retention was tested 48 h later with a series of two 30-s conditional auditory stimuli. For contextual fear extinction, mice were placed for 3 min in the contextual fear recall context every 24 h for five consecutive days starting the day after contextual fear recall. Contextual fear retention was tested 48 h after the last extinction session. For each trial, a camera recorded mice behaviour. A double-blind evaluation of the freezing time was achieved live and then *post hoc* using the videos.

### Fear generalization

One week after fear conditioning and extinction sessions, a second fear conditioning trial was achieved with two sequences of 28-s 2.5-kHz tone (conditional stimulus, repetition frequency: 440 Hz, 75 dB) followed by a 2-s electric shock (0.8 mA, unconditional stimulus) in an original context (context A: original shape Plexiglas arena with red tape and a new odour atmosphere with limonene scent). Twenty-four hours after conditioning, mice were placed for five consecutive 3-min trials successively in context A, context B (different  $20 \times 20$  cm cage, with a smooth floor in Plexiglas but same olfactory cue ([+]-limonene)), context C (same cage as context B but without the odour, with an auditory 7.5 kHz conditional stimulus), context D (same cage as context B but with a new odour ([-]-carvone)), and context A again to measure extinction. Each 3-min context exposure was separated by an inter-trial period of 1 min where the mouse was placed in its home cage. For each trial, a camera recorded mice behaviour. A double-blind evaluation of the freezing time was achieved live and *post hoc* using the videos.

### Immunohistochemistry

Mice were euthanized by an intracardiac infusion of 0.9% NaCl and 4% Formol under deep anaesthesia (xylazine 20 mg/kg, ketamine 100 mg/kg). Brains were extracted with forceps after incision of the skin and medial section of the skull with fine scissors. Brains were post-fixed with Formol 4% over night at  $4^\circ\text{C}$  (or only 2 h for c-fos labelling), then rinsed with phosphate-buffered saline (PBS) before being stored in PBS with 30% sucrose. Brains were then coronally cut into 60- $\mu\text{m}$  thick sections with a freezing microtome (Leica). The sections of interest were stored in PBS with 0.01% azide. The immunolabelling protocol begun with a permeabilization step using PBS with 0.2% Triton X-100 and 10% normal donkey serum (NDS, Abcam, Ab7475) blocking agent [or normal goat serum (NGS), Abcam, Ab7481; depending on the experiments] for 2 h under constant agitation. Primary antibodies diluted according to the supplier's recommendations were then incubated with PBS with 0.2% Triton (PBST), NDS 10% (or NGS) and azide 0.01%, at  $4^\circ\text{C}$  with constant agitation for a variable duration (between 1 and 4 days). Primary antibodies used were PKC $\delta$  (1:1000, mouse, BD Biosciences, 610398), SOM (1:500, goat, Santa Cruz, Sc-7819), c-fos (1:1000, rabbit, Santa Cruz, Sc-52/Ch; 1:1000, rabbit, Abcam, Ab190289), green fluorescent protein (GFP) (1:500, chicken, Abcam,

Ab13970) and red fluorescent protein (RFP) (1:4000, rabbit, Rockland, 600-401-379). After three 5-min washes with PBS, sections were incubated with either Alexa Fluor 488-, 568- or 647-conjugated secondary antibodies (Invitrogen, ThermoFisher) with PBST 0.2%, NDS 2% (or NGS 2%) and DAPI (0.01%) at room temperature with constant agitation for 2 h. After three 5-min washes with PBS, slices were mounted on slides with a mounting medium (FluoroMount-G, Interchim). Image acquisition was carried out either with an apotome microscope (Zeiss), a confocal microscope (LSM 700, Zeiss) or a digital slide scanner (Axio Scan, Zeiss), according to the experiments. Quantification of c-fos+ neurons was achieved using the 'spot detection' function of ICY software (Institut Pasteur, France Bioimaging), allowing counting of the number of c-fos+ cells in brain areas previously drawn on the slides' images via the region of interest function of the same software. For analysis of rabies virus-labelled neurons, 60- $\mu$ m thick coronal sections were cut and one section out of three was serially collected for RFP/DAPI staining before mounting. We analysed sections from the anterior insular cortex to the end of the brainstem, based on the Paxinos atlas.<sup>46</sup> mCherry-positive somas were counted from all selected slices except for regions surrounding the rabies virus injection (~300  $\mu$ m radius), due to the reported non-specific expression of virus at the site of injection.<sup>50</sup> The fraction of total presynaptic neurons for each animal was obtained by dividing the number of mCherry+ somas for each brain region by the total number of somas counted in the entire hemisphere, to then produce a colour-coded map. Regions with less than 1% of total cells were not further represented. All BNST subregions were pooled, except the oval nucleus.

### RNA purification and quantification by quantitative PCR

Whole brain for RNA analysis was collected in liquid nitrogen and stored at  $-80^{\circ}\text{C}$  before processing. Tissues were thawed in 1 ml of Qiazol (Qiagen) then shredded using a TissueLyzer II and metallic beads (Qiagen). Two hundred microlitres of chloroform (Merck) were added before spinning for 15 min at  $4^{\circ}\text{C}$ , 20 000g. The upper aqueous phase was collected for RNA purification and quantification. Total nucleic acid from the whole brain was purified using RNEasy Minikit with a DNase step (Qiagen) to remove any remaining genomic DNA. Purified RNA was quantified and a reverse transcription on 500 ng of RNA using SuperScript<sup>®</sup> II Reverse Transcriptase (Life Technologies) was performed. Quantitative PCR amplification was achieved on 500 pg of cDNA using StepOne Plus RealTime PCR system (Applied Biosystems) and SYBR Green PCR select master mix (Roche). Cycling conditions were  $50^{\circ}\text{C}$  for 2 min,  $95^{\circ}\text{C}$  for 10 min and 40 cycles of  $95^{\circ}\text{C}$  for 15 s and  $60^{\circ}\text{C}$  for 1 min. All experiments were performed in triplicate. The relative abundance of amplified cDNA was calculated as  $2^{-\Delta\text{Ct}}$ , where  $\Delta\text{Ct}$  (change in cycle threshold) equals Ct in the target gene minus Ct in the control gene. Results are expressed as the ratio of  $2^{-\Delta\text{Ct}}$  from the tested group to the control group. For the data presented in [Supplementary Fig. 1M](#), mice were perfused with 20 ml of PBS under deep anaesthesia (xylazine 20 mg/kg, ketamine 100 mg/kg). The brain was quickly removed and cooled down in cold PBS. Then a 2-mm<sup>2</sup> fragment containing the amygdala was cut and immediately put in RNAlater<sup>®</sup> solution (Sigma-Aldrich) and kept at  $4^{\circ}\text{C}$  until processing. RNA extraction was performed following the PureLink RNA Mini Kit protocol (ThermoFisher). Synthesis of cDNA was done using SuperScript IV (ThermoFisher) according to the manufacturer's instructions. Real-time quantitative PCR was performed using SYBR Green

and primers from Bio-Rad. Ct values were normalized to the mean Ct obtained with *Gapdh* and *Hsp90* as housekeeping genes.

### Cytokine multiplex

After blood collection in 1.5-ml tubes (Eppendorf), serum was obtained with centrifugation for 10 min at 9000g, immediately frozen in dry ice and stored at  $-80^{\circ}\text{C}$  until assay. Cytokines and chemokines were measured using Bio-Plex magnetic bead fluorescence measurements. Bio-Plex pro MT Mouse Cytokine Standard 23-Plex Group 1 kit (Bio-Rad) was used following the manufacturer's recommendations, which allow measurement of eotaxin, G-CSF, GM-CSF, IFN- $\gamma$ , IL-1 $\alpha$ , IL-1 $\beta$ , IL-2, IL-3, IL-4, IL-5, IL-6, IL-9, IL-10, IL-12 (p40), IL-12 (p70), IL-13, IL-17A, KC, MCP-1 (MCAF), MIP-1 $\alpha$ , MIP-1 $\beta$ , RANTES and tumour necrosis factor (TNF). Cytokine concentrations were normalized to the total protein concentration in each serum aliquot. Cytokines that did not reach the level of detection were not included in the analysis.

### Statistical analysis

All experiments and data analyses were achieved blinded unless otherwise stated. In the figures are indicated the number of subjects used in each experimental condition and the data are expressed as mean  $\pm$ SD (or  $\pm$ SEM if stated). Two-sided statistical analyses were performed with GraphPad Prism 6.0. No statistical methods were used to pre-determine sample size or to randomize. Samples normality was previously tested using the D'Agostino and Pearson omnibus normality test. For comparison of two means tests, an unpaired t-test was used if the sample passed the normality test, with Welch's correction if the compared groups' standard deviations were significantly different. If the sample did not pass the normality test, we used the Mann-Whitney test. For statistical analysis between three or more independent groups, we used ANOVA tests coupled to *post hoc* Sidak's multiple comparison tests. In behavioural experiments, outliers were identified using Grubbs' method ( $\alpha=0.05$ ) and then removed. For correlation analysis, we use the Pearson test. Statistical significance was set at \* $P < 0.05$ , \*\* $P < 0.01$ , \*\*\* $P < 0.001$ , \*\*\*\* $P < 0.0001$ .

### Data availability

The datasets generated during the current study as well as the custom code used to analyse the data are available from the corresponding authors upon reasonable request.

## Results

### CLP mice develop long-term anxiety and PTSD-like conditioned fear expression

To assess the neurobiological mechanisms of long-term behavioural disorders following sepsis, we used the validated murine model of sepsis induced by peritonitis after CLP.<sup>27</sup> We confirmed that this model reproduces the major features of human sepsis, including a severe systemic and brain inflammatory response and transient neuroinflammation as assessed by increased expression of circulating cytokines and brain mRNA coding for IL-1 $\beta$  and TNF ([Fig. 1A and B](#) and [Supplementary Fig. 1A](#)). CLP was also associated with sickness behaviour ([Fig. 1C](#)), sleep alterations characterized by sleep fragmentation with frequent arousal<sup>27,28</sup> as well as EEG abnormalities, characterized by slower rhythms and power decrease ([Supplementary Fig. 1C](#)). This EEG feature is classically observed in human sepsis patients<sup>5</sup> and is thought to be a consequence of

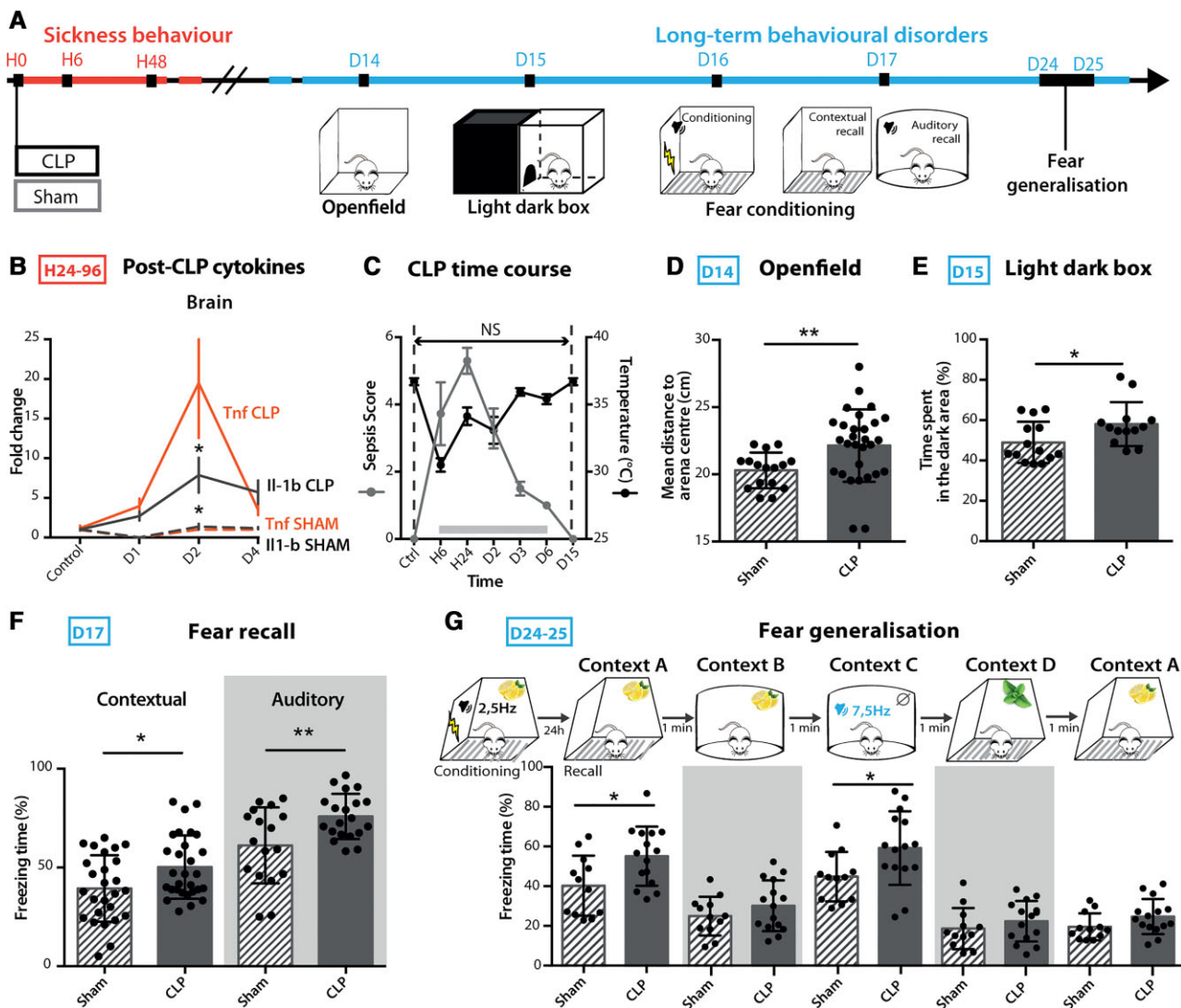


**Figure 1** CLP mice developed long-term anxiety and PTSD-like conditioned fear expression. (A) Timeline of the experiment: long-term anxiety and fear-related behaviours were tested from 2 weeks post-surgery. (B) Brain cytokine levels were significantly increased post-CLP [ $n_{\text{control}} = 5$ ,  $n_{\text{D1-sham}} = 1$ ,  $n_{\text{D1-CLP}} = 5$ ,  $n_{\text{D2-sham}} = 4$ ,  $n_{\text{D2-CLP}} = 8$ ,  $n_{\text{D3-sham}} = 5$ ,  $n_{\text{D3-CLP}} = 5$ . IL1-b: group  $F(1,30) = 2.931$ ,  $P = 0.0972$ , D2:  $*P = 0.0119$ ; TNF: group  $F(1,30) = 7.354$ ,  $*P = 0.0110$ , D2:  $*P = 0.0141$ ]. (C) CLP-induced sickness behaviour ( $n_{\text{control}} = 9$ ,  $n_{\text{CLP}} = 90$ ) was transient and totally disappeared at D15. (D and E) CLP caused long-term anxiety behaviour illustrated by an increased mean distance to arena centre in the open field (D;  $n_{\text{sham}} = 16$ ,  $n_{\text{CLP}} = 23$ ,  $**P = 0.0037$ ) and an increased time spent in the dark area during the light/dark box test (E;  $n_{\text{sham}} = 14$ ,  $n_{\text{CLP}} = 13$ ,  $*P = 0.0348$ ). (F) Twenty-four hours after aversive conditioning, CLP mice displayed an enhanced freezing behaviour during both contextual and auditory fear conditioning recall (Contextual:  $n_{\text{sham}} = 27$ ,  $n_{\text{CLP}} = 29$ ,  $*P = 0.0176$ ; Auditory:  $n_{\text{sham}} = 18$ ,  $n_{\text{CLP}} = 20$ ,  $*P = 0.0108$ ). (G) CLP mice showed an increased freezing behaviour when confronted to stimuli partially related to the conditional stimulus in the generalization test [ $n_{\text{sham}} = 12$ ,  $n_{\text{CLP}} = 15$ , group,  $F(1,25) = 9.243$ ,  $**P = 0.0055$ ; Context A,  $*P = 0.0136$ ; Context C,  $*P = 0.0183$ ]. Statistics: (D–F) Mann–Whitney test or unpaired t-test; (B, C and G) two-way ANOVA and Sidak’s multiple comparison tests (grey bar when significant). Data shown as mean  $\pm$  SD. D = days post-surgery; H = hours post-surgery.

the sepsis-induced decrease of cerebral blood flow and metabolism.<sup>51</sup> CLP lethality was approximately 50% (Supplementary Fig. 1B). A sepsis score using clinical and behavioural criteria was set to regularly evaluate over time the symptoms developed post-surgery. CLP mice were compared to sham animals that only underwent a laparotomy procedure with the same anaesthetic and analgesic protocol as CLP mice, or control-naïve animals that only underwent the same anaesthetic and analgesic protocol. Fifteen days post-CLP (D15), mice that recovered from sepsis showed no sign of remaining sickness behaviour (Fig. 1A–C and Supplementary Fig. 1A). However, these mice displayed enhanced anxiety, with a significant avoidance of the arena centre in the

open field test (Fig. 1D) and an increased time spent in the dark arena in the light/dark box test (Fig. 1E) when compared to sham mice. In addition to anxiety-like spontaneous avoidance behaviours, we also assessed fear memory in CLP recovered mice using a contextual and auditory fear conditioning paradigm, in which an electric foot shock (aversive unconditional stimulus) is paired with a discrete auditory cue in a specific context (conditioned stimulus).<sup>23,52</sup> Twenty-four hours after the acquisition phase, we monitored the fear memory retrieval, assessed by context- or tone-induced freezing behaviour. CLP mice showed an increased freezing time in both the contextual and auditory recalls (Fig. 1F), despite exhibiting a similar behaviour to sham animals during the acquisition phase



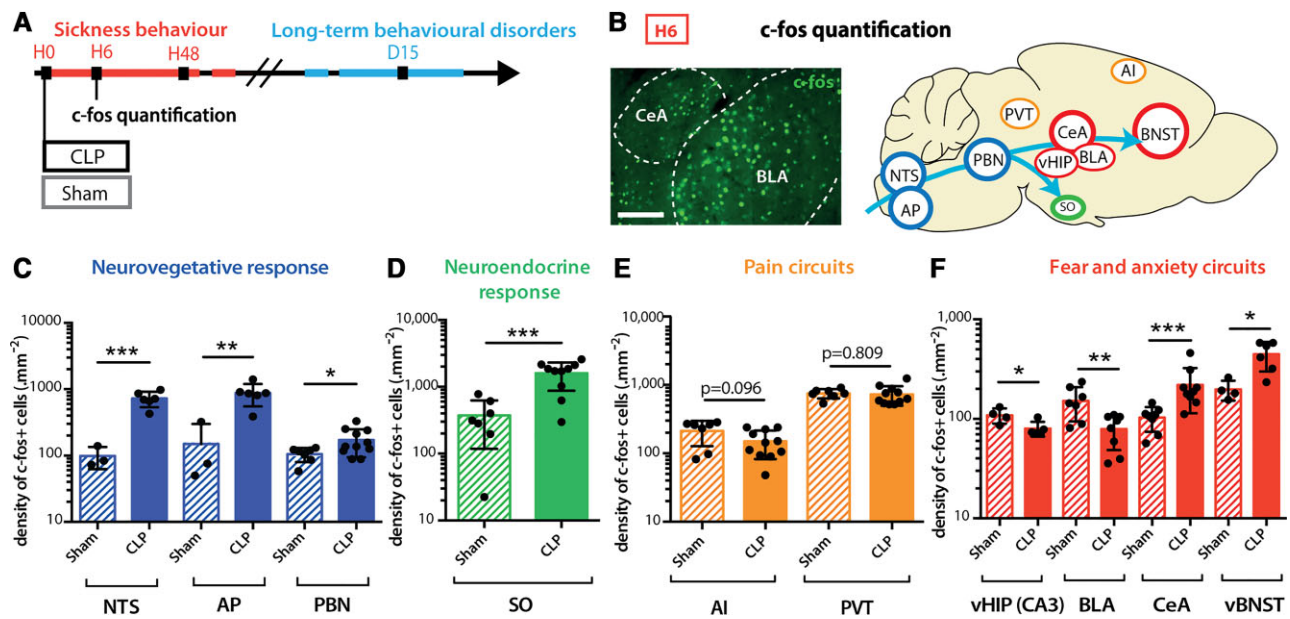


**Figure 2** CLP induced transient brain activation. (A and B) Neuronal activation marker c-fos was quantified at H6 post-surgery. Scale bar = 200  $\mu\text{m}$ . (C and D) H6 c-fos quantification showed transient neuronal activation in CLP compared to sham mice in areas involved in the neurovegetative response [C; NTS:  $n_{\text{sham}}=3$ ,  $n_{\text{CLP}}=6$ ,  $***P=0.0009$ ; area postrema (AP):  $n_{\text{sham}}=3$ ,  $n_{\text{CLP}}=6$ ,  $**P=0.0089$ ; PBN:  $n_{\text{sham}}=7$ ,  $n_{\text{CLP}}=12$ ,  $*P=0.0255$ ] and the neuroendocrine system [D; supra-optic nucleus (SO):  $n_{\text{sham}}=7$ ,  $n_{\text{CLP}}=10$ ,  $***P=0.0003$ ]. (E) At H6, CLP showed no effect on the activation of pain related areas compared to the sham group [agranular insular area (AI), paraventricular nucleus of the thalamus (PVT)  $n_{\text{sham}}=7$ ,  $n_{\text{CLP}}=11$ ]. (F) CLP-induced c-fos expression variations at H6 in areas involved in fear and anxiety circuits [ventral hippocampus (vHIP) cornu ammonis 3 (CA3):  $n_{\text{sham}}=4$ ,  $n_{\text{CLP}}=5$ ,  $*P=0.0328$ ; BLA:  $n_{\text{sham}}=7$ ,  $n_{\text{CLP}}=8$ ,  $**P=0.0079$ ; CeA:  $n_{\text{sham}}=8$ ,  $n_{\text{CLP}}=9$ ,  $***P=0.0006$ ; vBNST:  $n_{\text{sham}}=4$ ,  $n_{\text{CLP}}=6$ ,  $*P=0.0121$ ]. Statistics: (C–F) Mann–Whitney test or unpaired t-test. Data shown as mean  $\pm$  SD.

(Supplementary Fig. 1F). This facilitated freezing response was also detected for auditory stimulus that had not been previously paired with the conditioned stimulus (Fig. 1G). On the contrary, contextual fear generalization was similar to sham animals (Fig. 1G), indicating that CLP mice display only a partial fear generalization to auditory cues. We observed only a limited deficit in fear extinction, with a non-significant trend towards higher freezing responses in CLP mice tested for short-term spontaneous recovery of fear retention following repeated presentations of the conditioned stimulus (Supplementary Fig. 1G). These exaggerated fear responses did not result from a diminished pain threshold (monitored as motor reactivity to the shock, Supplementary Fig. 1F) and were no longer observed 45 days post-sepsis (Supplementary Fig. 1H). In contrast to fear memory, CLP mice did not show any impairment of either recognition memory—assessed by novel object recognition test (Supplementary Fig. 1J) and olfactory habituation–dishabituation tests (Supplementary Fig. 1K)—or spatial contextual learning—assessed both by novel object localization (Supplementary Fig. 1J) and Morris water maze (Supplementary Fig. 1I). Lastly, long-term fear impairments at D15 positively correlated with the magnitude of the sepsis score (maximum score between H24 and H48), which also correlated with the brain expression level of cytokines and chemokines at H48 (Supplementary Fig. 1L and M). Together these results demonstrate that 15 days after CLP-induced sepsis, mice exhibit both anxiety in spontaneous exploration tests and exacerbated PTSD-like conditioned fear response with partial fear generalization.

### CLP induces transient brain activation

To decipher the origin of the sepsis-induced long-term behavioural alterations, we characterized the brain activity changes during the

acute phase of sepsis. The expression level of the neuronal activation marker gene c-fos was monitored during the 24 h following sepsis (Fig. 2A and B and Supplementary Fig. 2A). At 6 h (H6) post-CLP, c-fos expression was increased in nuclei of the autonomic, vagal and neuroendocrine systems such as the nucleus of the solitary tract (NTS), the area postrema (AP), the PBN and the supraoptic nucleus of the hypothalamus (Fig. 2C and D). The lack of significant activation in areas strictly involved in pain perception, such as the paraventricular thalamus and the agranular insular cortex, ruled out any contribution of nociception to the sepsis-induced brain activation (Fig. 2E). Remarkably, a high level of c-fos protein was observed in brain regions classically involved in fear and anxiety, with a transient activation in the CeA and the vBNST, and decreased activity in the ventral hippocampus and the BLA (Fig. 2F).<sup>53</sup> Those activated brain regions—converging on the CeA—are known to be involved in feedback loops orchestrating defensive behaviour.<sup>15,16,54</sup> This activation pattern at H6 was transient and returned to baseline levels at H24 (Supplementary Fig. 2B–E).

### CLP triggers the activation of PKC $\delta$ <sup>+</sup> CeA neurons projecting to the vBNST and the substantia innominata

To characterize the neuronal populations of the CeA transiently activated during sepsis, we performed co-immunolabelling with markers of CeA subpopulations. c-Fos-positive (c-fos<sup>+</sup>) CeA neurons primarily expressed PKC $\delta$  and did not co-localize with SOM (Fig. 3A). We then labelled these c-fos<sup>+</sup> neurons by injecting into the CeA a Cre-dependent GFP-positive adeno-associated virus (AAV) into transgenic mice expressing the tamoxifen-inducible Cre-recombinase enzyme under the control of the c-fos promoter.<sup>43</sup> Three hours after CLP, tamoxifen was injected, restricting the

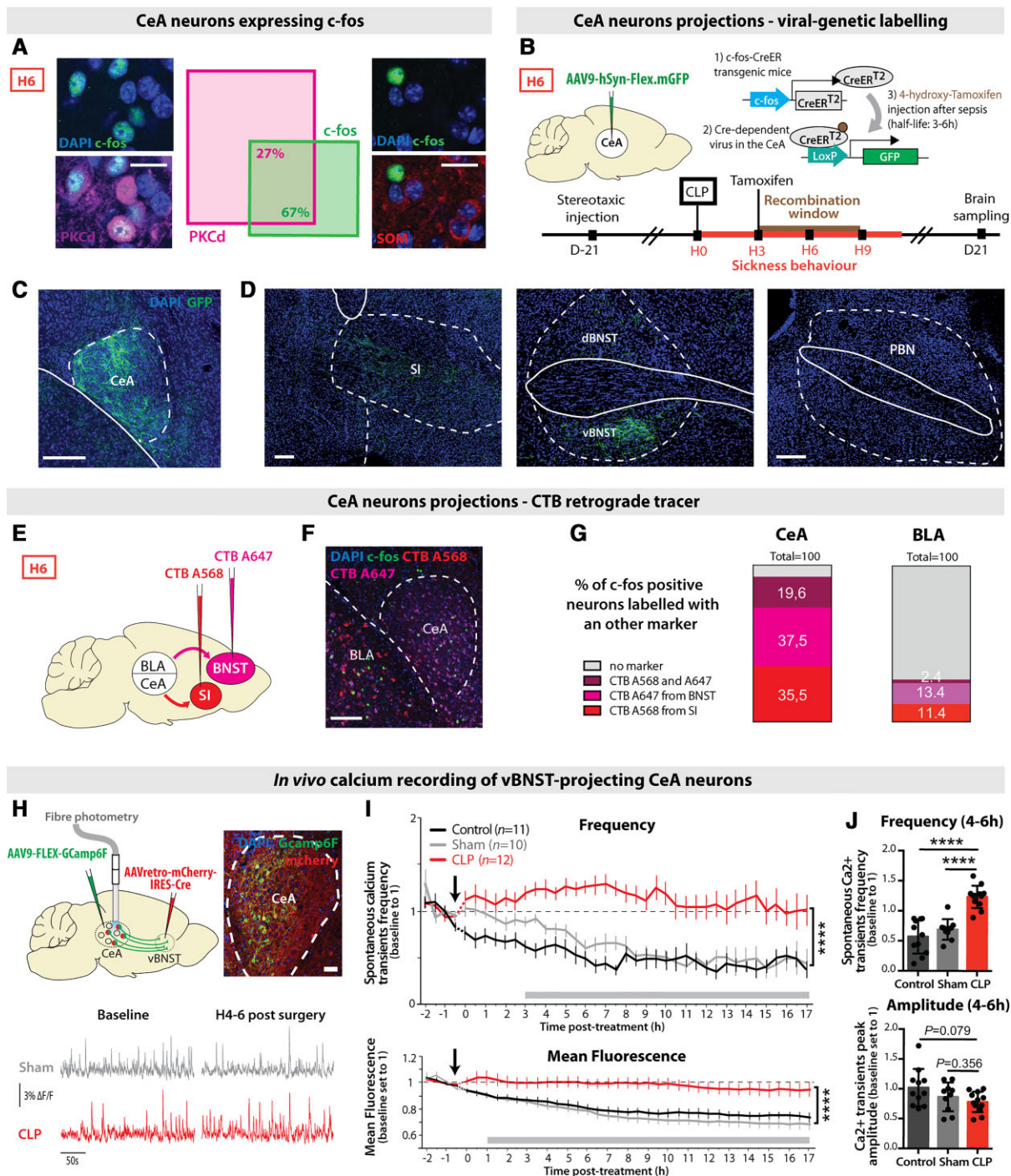


**Figure 3** CLP triggered the activation of PKC $\delta$ <sup>+</sup> CeA neurons projecting to the vBNST and the substantia innominata. (A) CeA c-fos<sup>+</sup> neurons at H6 post-CLP were 67% co-localizing with PKC $\delta$ <sup>+</sup> neurons, but 0% with SOM<sup>+</sup> neurons ( $n=6$ , total cell counted,  $n_{c-fos+/PKC\delta} = 301/453$ ,  $n_{c-fos+/SOM} = 0/144$ ; scale bar = 20  $\mu\text{m}$ ). (B–D) Viral trapping of CeA c-fos<sup>+</sup> neurons at H6. (B) A Cre-dependent GFP<sup>+</sup> AAV virus was injected in the CeA of transgenic mice expressing the tamoxifen-inducible Cre-recombinase enzyme under the control of the c-fos gene promoter. 4-Hydroxy-tamoxifen was injected into these mice 3 h after CLP for restricting the recombination window between H3 and H9 post-CLP. (C) Recombination site in the CeA. Scale bar = 200  $\mu\text{m}$ . (D) GFP<sup>+</sup> fibres only projected to the vBNST and the substantia innominata (SI) but not to other reported projection regions of CeA PKC $\delta$ <sup>+</sup> neurons such as the PBN ( $n=3$ , scale bar = 200  $\mu\text{m}$ ). (E–G) CTB retrograde tracing. (E) CTB A568 was injected in the substantia innominata and CTB A647 in the BNST. Mice underwent a CLP surgery 5 days after stereotaxic injection and were sacrificed at H6. (F) Representative picture of c-fos<sup>+</sup> staining and CTB labelling. (G) C-fos<sup>+</sup> neurons colocalized at 92.6% with retrograde CTB A568 and/or CTB A647 tracers in the CeA. In a control region such as the BLA, only 27.2% of the H6 c-fos<sup>+</sup> neurons were co-localizing with both CTB tracers ( $n=3$ , total cell counted,  $n_{c-fos} = 173$ , scale bar = 200  $\mu\text{m}$ ). (H–J) *In vivo* calcium imaging of vBNST-projecting CeA neurons. (H) Gcamp6f-specific expression and recordings in the vBNST-projecting CeA neurons (scale bar = 50  $\mu\text{m}$ ) before and after surgery (CLP, red; sham, grey). (I) Spontaneous calcium events frequency (top) and mean fluorescence (bottom) in the vBNST-projecting CeA neurons were higher in CLP compared to control or sham mice [frequency: interaction:  $F(76,1075) = 2.268$ ; group:  $F(2,1075) = 381.6$ , \*\*\*\* $P < 0.0001$ ; mean fluorescence: interaction:  $F(76,1107) = 1.602$ ,  $P = 0.0011$ ; group:  $F(2,1107) = 336.1$ , \*\*\*\* $P < 0.0001$ ]. (J) Between H4 and H6 ( $n_{\text{Control}} = 11$ ,  $n_{\text{Sham}} = 10$ ,  $n_{\text{CLP}} = 12$ ), CLP mice (compared to control or sham animals) displayed a higher frequency of calcium events with a non-significant decrease in amplitude of those events. Statistics: (I) Two-way ANOVA and Sidak's multiple comparison tests (grey bar when significant). (J) Mann-Whitney test or unpaired t-test, \*\*\*\* $P < 0.0001$ . Data shown as mean  $\pm$  SEM (I) and mean  $\pm$  SD (J).

recombination window around H6 (Fig. 3B). Labelled CeA neurons (Fig. 3C) exclusively projected to the vBNST and the substantia innominata (Fig. 3D and Supplementary Fig. 3A), two pallidal regions involved in emotional encoding.<sup>55–57</sup> Labelled CeA neurons did not project to the other reported output regions of the PKC $\delta$ <sup>+</sup> CeA neurons, like PBN (Fig. 3D and Supplementary Fig. 3A).<sup>58</sup> To confirm these results, we retrospectively labelled CeA neurons projecting to the substantia innominata and BNST with two different retrograde CTB tracers (Fig. 3E and F) and observed that a vast majority of c-fos<sup>+</sup> CeA neurons at H6 post-CLP co-localized with these CTB markers (Fig. 3G). Considering that vBNST is highly activated post-sepsis and is involved in anxiety-related disorders,<sup>25,59</sup> we targeted the expression of the fluorescent calcium reporter GCaMP6f in vBNST-projecting CeA neurons. For this, we injected in the vBNST a retrograde Cre-expressing virus and in the CeA a conditional Cre-dependent virus expressing GCaMP6f. Finally, we implanted an optic fibre above the CeA to chronically monitor the activity of vBNST-projecting CeA neurons before and after CLP (Fig. 3H). CLP induced a rapid and sustained increase in the frequency of spontaneous population calcium transients as well as in the mean fluorescence intensity (Fig. 3I), compared to sham and control animals. Corroborating the c-fos gene expression data, this effect was already visible at H4–H6 (Fig. 3J). The increased frequency of calcium events following CLP was associated by a slight decrease in mean peak amplitude (Fig. 3J). Altogether, these data revealed that brain regions involved in anxiety and fear expression are activated during the acute phase of sepsis, with an important activation of a subpopulation of PKC $\delta$ <sup>+</sup> CeA neurons projecting to the vBNST. Given that in humans, epileptic discharges are observed in a significant proportion of sepsis patients, we also performed *in vivo* LFP recordings in the CeA (Supplementary Fig. 3B). Following CLP, seizure or epileptic sharp-wave discharges were absent in the CeA. However, the transient occurrence of some large isolated stereotyped epileptiform-like spikes was observed in 20% of the animals within 1 to 4 h following CLP, indicative of the potential emergence of focal epileptic-like abnormalities in the amygdala during the sepsis acute phase (Supplementary Fig. 3B and C).

### CLP induces long-term alterations of synaptic connectivity and functional activity of vBNST-projecting CeA neurons

To understand how sepsis imprinted durable anatomical and functional changes in brain circuits at D15, we investigated the impact of CLP on the presynaptic connectivity of the vBNST-projecting CeA neurons, using targeted retrograde rabies virus-based monosynaptic tracing. In this approach, we restricted the rabies infection only to vBNST-projecting CeA neurons with a retrograde Cre-expressing virus injected in the vBNST and, in the CeA, a conditional Cre-dependent ‘helper’ virus to express the avian tumor virus receptor A (TVA) and the rabies glycoprotein. Three weeks later, injected animals were divided into two groups and experienced either CLP or sham surgery. Two weeks post-surgery, we injected a glycoprotein-deleted EnvA-pseudotyped mCherry-expressing rabies virus [(EnvA)SAD- $\Delta$ G-mCherry] that only infected neurons expressing TVA receptors and spread only from cells expressing the glycoprotein. Six days post-injection, we examined sections of the entire brain to quantify the location and the relative number of mCherry-positive neurons (Fig. 4A and B). To visualize the connectivity map of presynaptic neurons to vBNST-projecting CeA neurons, we generated a map of the relative proportion of each brain region in the control condition (showing regions with >1% total

inputs). Labelled brain regions directly projecting onto CeA neurons were similar to those reported previously for PKC $\delta$ <sup>+</sup> CeA neurons,<sup>22</sup> with major inputs originating from midbrain (PBN, retrorubral field), cortical regions (BLA, agranular insular cortex, post-piriform transition area), hypothalamus (lateral hypothalamic area, ventromedial hypothalamic nucleus) and BNST (Fig. 4C). By comparing CLP to sham mice, we established a map of the differential contribution of input regions. This brain map revealed which regions exhibit a distinct connectivity pattern at D15 post-CLP (relative to sham). We observed that BNST (including the ON) and the midbrain dopaminergic region retrorubral field—two regions involved in threat and aversive signal processing—contained fewer labelled neurons in the CLP group (Fig. 4D).

To complement to this anatomical characterization, we investigated the functional activity of vBNST-projecting CeA neurons at D15 during behavioural tests. To express the calcium reporter Gcamp6f in the CeA neurons projecting to the vBNST, we used the same genetic design as described in Fig. 3 in both CLP and sham mice (Fig. 4E). We performed *in vivo* fibre photometry recordings of those neurons during auditory fear conditioning and fear recall at D15 (Fig. 4E). During the learning phase, CeA neuronal activity did not significantly change in response to the auditory conditioned stimulus (Fig. 4F), but exhibited a strong excitatory response to foot shock, without any difference between CLP and sham animals (Fig. 4G). During fear recall, we observed that the conditioned stimulus induced a significant inhibitory response in CLP mice compared to sham animals (Fig. 4H), as previously reported in PKC $\delta$ <sup>+</sup> CeA neurons.<sup>60</sup> Thus, at D15 post-CLP, vBNST-projecting CeA neurons exhibited an altered synaptic connectivity and a marked responsiveness to the conditioned stimulus.

### LEV administration during sepsis suppresses the transient neuronal activation in vBNST-projecting CeA neurons

Considering that the acute brain response to CLP was characterized by the transient hyperactivation of specific circuits, associated with epileptic-like abnormalities, we hypothesized that the sepsis-induced transient activation of brain anxiety circuits could be responsible for the long-term PTSD-like condition fear expression. To test this hypothesis and implement a potential preventive therapeutic approach aiming at alleviating the emergence of long-term anxiety-related behaviours,<sup>61,62</sup> we evaluated the effect of the neuromodulatory and anti-epileptic drug LEV. To test its impact on sepsis-induced brain hyperactivation in our CLP model, we administered LEV by intraperitoneal injection immediately after surgery (Fig. 5A). LEV administration at H0 prevented the transient neuronal c-fos gene expression observed at H6 in CLP mice specifically in the extended amygdala (CeA and vBNST) and the vagal system (NTS and AP; Fig. 5B) and had nearly no effect in control mice (Supplementary Fig. 4A). Analysis of the blood cytokines in CLP animals treated with LEV indicated that LEV had no peripheral anti-inflammatory effects (Supplementary Fig. 4B). *In vivo* calcium imaging of the vBNST-projecting CeA neurons showed that LEV suppressed the transient sepsis-induced increase in the frequency of spontaneous calcium transients while restoring the mean peak amplitude of these transients (Fig. 5C–E). To further characterize the activity-dependent effect of LEV in the amygdala circuits, we monitored the evoked population activity of vBNST neurons in response to optogenetic activation of CeA axonal terminals 30 min following LEV intraperitoneal administration (Fig. 5F). Light stimulation at different frequencies revealed that LEV significantly

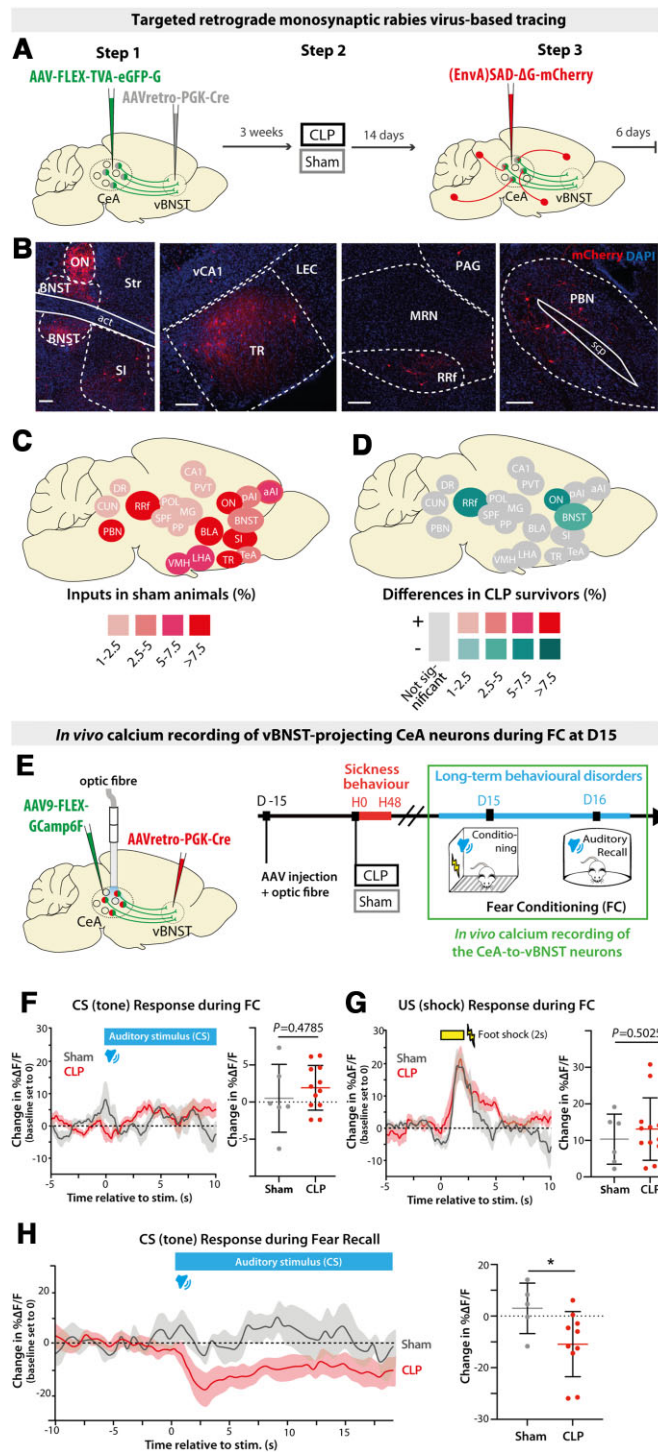


**Figure 4** CLP induces long-term alterations of synaptic connectivity and functional activity of vBNST-projecting CeA neurons. (A) Experimental design for targeting mCherry-expressing pseudotyped rabies virus to CeA neurons projecting to the vBNST in sham versus CLP survivors, 2 weeks after surgery. (B) Trans-synaptically labelled neurons in different brain regions. Scale bar = 100 μm. (C) Map of the brain regions providing the largest fraction of presynaptic neurons to the vBNST-projecting CeA neurons in sham animals (relative to the total). Regions providing <1% of total inputs are not displayed (n = 4). BNST included all BNST subdivisions except oval nucleus (ON). (D) Map of the differences in presynaptic neurons to vBNST-projecting CeA neurons in CLP survivors compared to sham survivors. Only regions showing significant difference are colour-coded (n<sub>CLP</sub> = 4, Mann-Whitney tests; BNST: \*P = 0.028, ON: \*P = 0.017, \*RRF: P = 0.049). (E) vBNST-projecting CeA neurons were chronically recorded during fear conditioning at D15 using fibre photometry. (F and G) Averaged ΔF/F traces (baseline set to 0) showing the responses to conditioned stimulus [tone; conditioned stimulus (CS); F] and unconditional stimulus [foot shock; unconditional stimulus (US); G] during fear conditioning in CLP and sham mice (n<sub>Sham</sub> = 6, n<sub>CLP</sub> = 12). Mean ΔF/F changes relative to baseline during the conditioned stimulus response (0–5 s window) and during the unconditional stimulus response (0–4 s window) showed no difference between CLP and sham mice. (H) Averaged ΔF/F traces (baseline set to 0) during fear conditioning (FC) recall exhibited a stronger inhibitory response to conditioned stimulus in CLP mice compared to sham animals (n<sub>Sham</sub> = 5, n<sub>CLP</sub> = 10, \*P = 0.0426). Statistics: (D and F–H) Mann-Whitney tests. Data shown as mean ± SD (except traces in F–H ± SEM). aAI = anterior agranular insular cortex; CUN = cuneiform nucleus; DR = dorsal raphe nucleus; LEC = lateral entorhinal cortex; LHA = lateral hypothalamic area; MG = medial geniculate nucleus; MRN = midbrain reticular nucleus; OV = oval nucleus; PAG = periaqueductal grey; pAI = posterior agranular insular cortex; POL = posterior limiting nucleus of the thalamus; PP = peripeduncular nucleus; RRF = retrorubral field; SPF = subparafascicular nucleus; TeA = temporal association area; TR = post-piriform transition area; vCA1 = ventral CA1; VMH = ventro-medial hypothalamic nucleus.

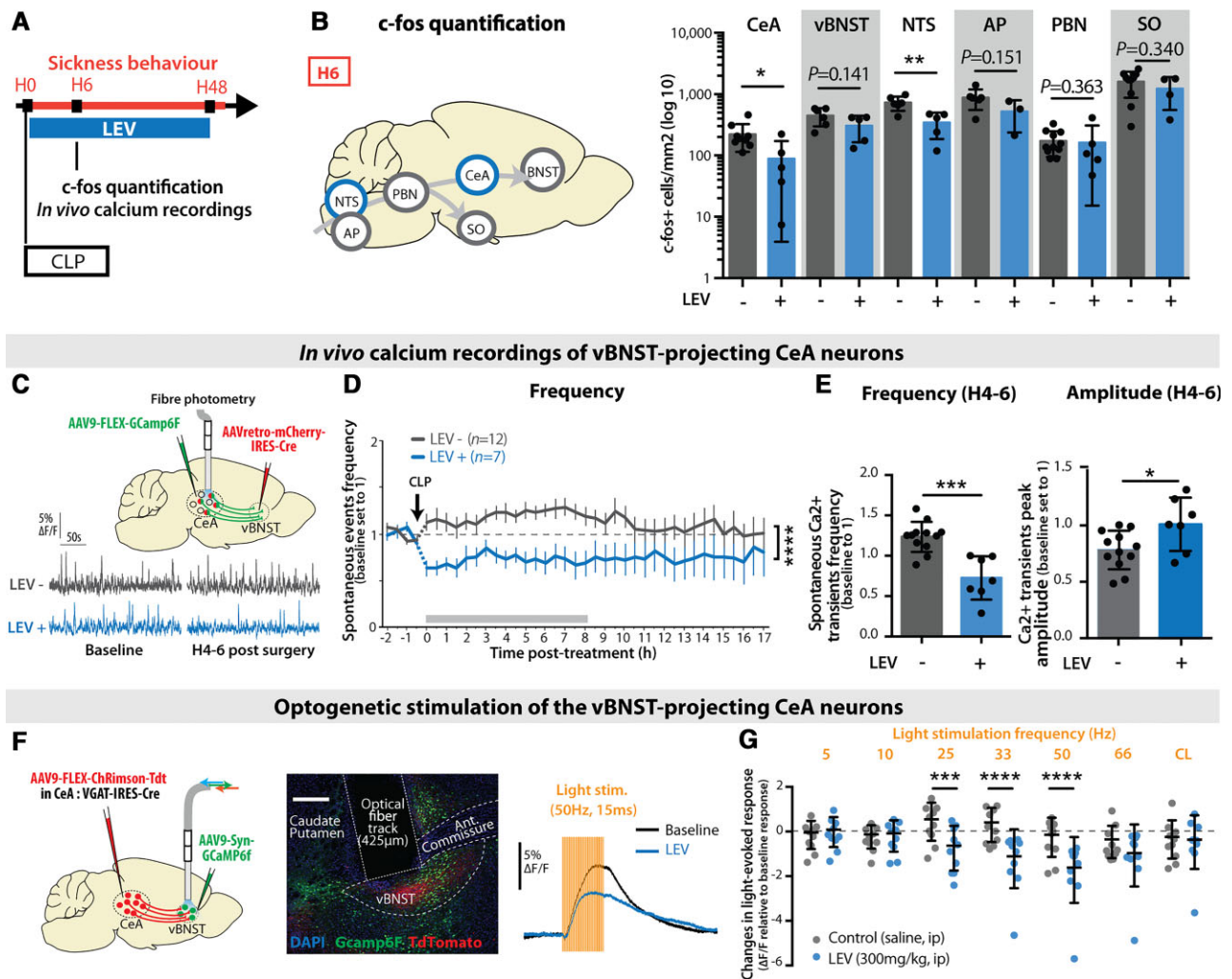


**Figure 5** LEV administration during sepsis suppressed the transient neuronal activation in vBNST-projecting CeA neurons. (A) LEV was administered every 12 h for 48 h post-CLP. (B) LEV treatment reduced the transient c-fos expression increase at H6 post-CLP only in the NTS and the CeA (CeA:  $n_{\text{CLP}}=9$ ,  $n_{\text{CLP}+\text{LEV}}=5$ ,  $^*P=0.0347$ , vBNST:  $n_{\text{CLP}}=6$ ,  $n_{\text{CLP}+\text{LEV}}=5$ ; NTS:  $n_{\text{CLP}}=6$ ,  $n_{\text{CLP}+\text{LEV}}=5$ ,  $^{**}P=0.0057$ ; AP:  $n_{\text{CLP}}=6$ ,  $n_{\text{CLP}+\text{LEV}}=3$ ; PBN:  $n_{\text{CLP}}=11$ ,  $n_{\text{CLP}+\text{LEV}}=5$ ; supra-optic nucleus (SO):  $n_{\text{CLP}}=10$ ,  $n_{\text{CLP}+\text{LEV}}=4$ ). (C–E) *In vivo* calcium imaging of the vBNST-projecting CeA neurons. (C) Gcamp6f specific expression and *in vivo* recording in the vBNST-projecting CeA neurons before and hours after CLP, in absence or presence of LEV treatment. (D) LEV administration showed a direct inhibiting effect over the increased neuronal spontaneous activity observed *in vivo* post-CLP [group:  $F(1,616)=141.7$ ,  $^{****}P<0.0001$ ]. (E) Between H4 and H6 post-CLP ( $n_{\text{CLP}}=12$ ,  $n_{\text{CLP}+\text{LEV}}=7$ ), LEV treatment induced a decreased frequency and an increased amplitude of the calcium events compared to non-treated animals (frequency:  $^{***}P=0.0001$ , amplitude:  $^*P=0.0265$ ). (F and G) Optogenetic stimulation of the axon terminals from ChRimsonR-expressing vBNST-projecting CeA neurons and recording of the light-evoked response in vBNST neurons. Scale bar = 200  $\mu\text{m}$ . Thirty minutes following LEV intraperitoneal injection (blue), the light-evoked response (normalized to the baseline light-evoked response before injection) was decreased compared to saline injection (grey) [ $n$  per group = 10, interaction:  $F(6,54)=5.472$ ; frequency:  $F(6,54)=5.472$ ,  $^{***}P=0.0002$ ; group:  $F(1,9)=3.412$ ,  $P=0.0978$ ; Control-LEV: 25 Hz,  $^{***}P=0.0009$ ]. CL = continuous light. LEV data in B are pooled with CLP data from Fig. 2 and LEV data in D and E are pooled with CLP data from Fig. 3. Statistics: (B and E) Mann–Whitney test or unpaired t-test. (D and G) two-way ANOVA (repeated measure for G) and Sidak’s multiple comparison tests (grey bar when significant).  $^{****}P<0.0001$ . Data shown as mean  $\pm$  SD (except D  $\pm$  SEM).

decreased the light-evoked response at high frequencies (25–50 Hz) but had no effect for lower frequencies (5–10 Hz; Fig. 5G), indicating that LEV has an inhibitory impact preferentially on CeA-to-vBNST circuits exhibiting high-frequency activity.

### Transient LEV treatment during sepsis acute phase dampens the post-CLP long-term behavioural impairments

Given that LEV dampened sepsis-induced hyperactivation of the extended amygdala, we tested whether a transient administration of LEV, only during the acute phase of sepsis, could prevent onset of long-term behavioural changes seen 15 days post-CLP.

Mice treated with LEV every 12 h during 48 h post-CLP showed at D15 a decreased anxiety level (Fig. 6A and B). This treatment reduced the PTSD-like fear response 15 days post-CLP, with a strong beneficial effect over the auditory recall to fear conditioning but no effect on contextual fear recall (Fig. 6C). Importantly, such 48 h-long LEV administration had no effect on pain threshold, general locomotor activity, recognition memory or spatial contextual memory (Supplementary Fig. 4C–H), ruling out potential deleterious long-term side effects of the drug on behaviour or cognition. Moreover, a 48 h-long treatment with LEV showed no effect at D15 on the open field and fear conditioning long-term behaviour in control mice (Supplementary Fig. 4C and E). Lastly, intracerebroventricular infusion of LEV (0.1 mg/h) during the 48 h post-CLP

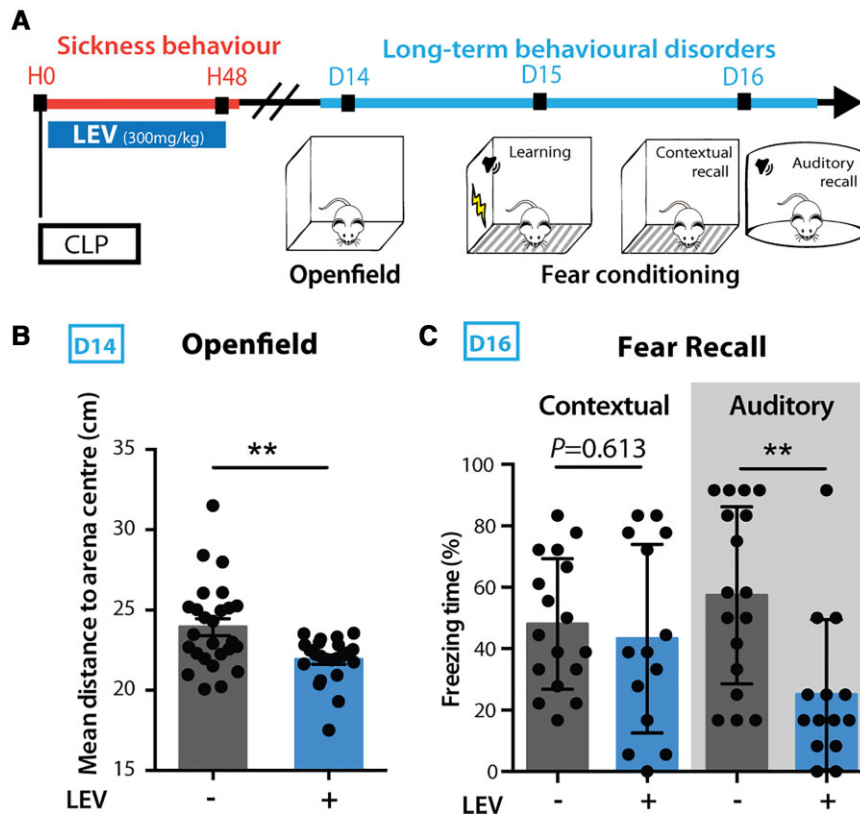


**Figure 6** Transient LEV treatment during sepsis acute phase dampened the post-CLP long-term behavioural impairments. (A) LEV was administered every 12 h during the first 48 h following CLP. Long-term behaviour was then tested 15 days post-CLP. (B and C) Early LEV administration decreased the mean distance to the open field arena centre (B;  $n_{\text{LEV}^-} = 26$ ,  $n_{\text{LEV}^+} = 22$ ,  $**P = 0.0055$ ) and the freezing behaviour during fear conditioning recall in CLP surviving mice (C;  $n_{\text{LEV}^-} = 17$ ,  $n_{\text{LEV}^+} = 14$ , Auditory:  $**P = 0.0024$ ). LEV data in B and C are pooled with CLP data from Fig. 1. Statistics: (B and C) Mann–Whitney test or unpaired t-test. Data shown as mean  $\pm$  SD.

showed no significant effects on the open field and the fear conditioning long-term behaviours in CLP mice (Supplementary Fig. 4I and J). Thus, we concluded that preventing early activation of fear- and anxiety-associated circuits during sepsis with an intraperitoneal administration of the inhibitory agent LEV strongly improved the psychocognitive outcomes of CLP mice.

### Transient pharmacogenetic silencing of vBNST-projecting CeA neurons prevents the development of anxiety and PTSD-like conditioned fear expression

To dissect the precise neuronal circuits involved in the generation of post-sepsis anxiety and PTSD-like fear expression, we performed a genetically encoded presynaptic transmitter release inhibition based on the conditional expression of the inhibitory Designer Receptor Exclusively Activated by Designer Drugs (DREADD).<sup>63</sup> We injected in the vBNST a retrograde Cre-expressing virus, and in the CeA a conditional Cre-dependent virus expressing the inhibitory hM4D(Gi) DREADD. This DREADD is only active when CNO is injected into the animal (Fig. 7A and B). The CNO was injected intraperitoneally at H0, H6, H12 and H24 post-surgery to induce 24 h transient inhibition of the targeted amygdala circuit. The c-fos staining confirmed that the pharmacogenetic silencing of synaptic transmission between CeA and vBNST prevented the CLP-induced neuronal activation at H6 in the post-synaptic region targeted by

hM4D(Gi)-expressing CeA neurons, i.e. the vBNST (Fig. 7C). Specific DREADD inhibition of the vBNST-projecting CeA neurons only during the 24 h post-CLP period prevented the development of anxiety and PTSD-like fear expression at D15 (Fig. 7D and E). Such transient silencing alleviates both anxiety in the open field test and auditory- and contextual-exaggerated fear responses during the fear conditioning test. In sham animals, DREADD-driven inhibition produced no behavioural changes (Supplementary Fig. 5A and B). These data confirmed that the sepsis-induced early activation of vBNST-projecting CeA neurons is necessary for the subsequent development of anxiety and PTSD-like fear expression.

## Discussion

In the present study, we have coupled circuit tracing techniques, *in vivo* imaging and targeted pharmacogenetic manipulation in mice to show that a transient pathological activation of a subpopulation of vBNST-projecting CeA neurons leads to the onset of long-term anxiety and PTSD-like fear expression. The dampening activity of this circuit prevents occurrence of these long-term post-sepsis adverse effects.

### CLP-induced sepsis as a new model of PTSD?

Despite the pathophysiological and clinical complexity of sepsis, several animal models have been developed in the field, ranging

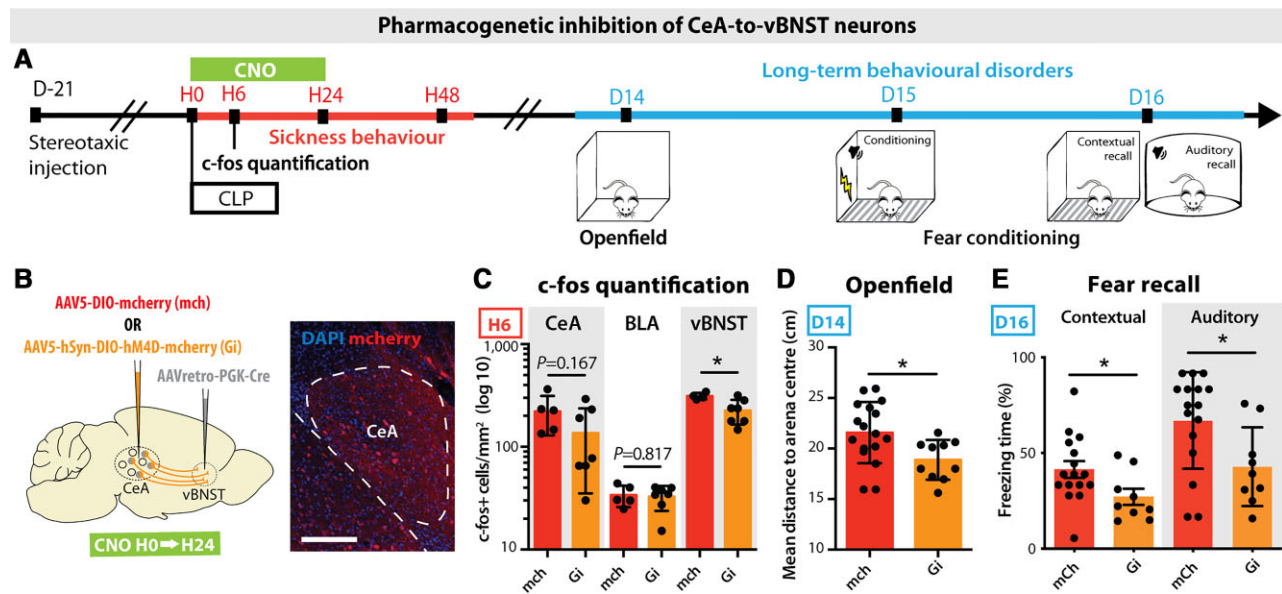


**Figure 7** Transient pharmacogenetic silencing of vBNST-projecting CeA neurons prevents the development of anxiety and PTSD-like conditioned fear expression. (A) Timeline of the experiment. Three weeks after stereotaxic injection of viral vectors, mice underwent a CLP and were injected with clozapine N-oxide (CNO) during the 24 h following surgery. Long-term behaviour was then tested 15 days post-surgery. (B) A retrograde Cre-expressing virus was injected in the vBNST and a Cre-dependent inhibitory DREADD (Gi) or mCherry control (mCh) virus was injected in the CeA to allow the recombination and the expression of the Gi/mCh viruses exclusively in the vBNST-projecting CeA neurons. (C) H6 c-fos quantification showed an inhibiting effect of Gi over the post-CLP neuronal activation in the vBNST compared to mCherry controls, with no impact on other neighbouring regions such as the BLA ( $n_{\text{mCh}} = 5$ ,  $n_{\text{Gi}} = 7$ , vBNST:  $*P = 0.0257$ ). (D and E) CNO-induced Gi inhibition for 24 h post-CLP is sufficient to abolish the long-term behavioural changes observed in the open field test (D;  $n_{\text{mCh}} = 17$ ,  $n_{\text{Gi}} = 10$ ,  $*P = 0.0190$ ) and the fear conditioning (FC) recall (E;  $n_{\text{mCh}} = 16$ ,  $n_{\text{Gi}} = 9$ , Contextual:  $*P = 0.0415$ ; Auditory:  $*P = 0.0228$ ). Scale bar = 200  $\mu\text{m}$ . Statistics: Mann-Whitney test or unpaired t-test. Data shown as mean  $\pm$  SD.

from administration of exogenous toxin (such as liposaccharide) to pathogen inoculation, or direct alteration of animal mucosal barriers. In this last category, CLP is the most commonly used model.<sup>26</sup> In mice, it leads to a syndrome strongly reminiscent of human sepsis. Indeed, contrary to liposaccharide or pathogen injection, CLP induces a polymicrobial infection with a large spectrum of the host intestinal microbiota, which recreates the major features of human sepsis acute phase, notably the characteristic cytokine storm.<sup>64</sup> In our study, we have shown a strong and quick increase of several peripheral pro- and anti-inflammatory cytokines (IL-1 $\alpha$ , IL-6, TNF, IL-10). This both pro- and anti-inflammatory cytokine profile and the kinetics of cytokine release is very similar to sepsis patients.<sup>57,58</sup> In agreement with previous reports, we also observed a transient neuroinflammatory response with brain expression of inflammatory cytokines and chemokines.<sup>34,65</sup> Additionally, CLP mice showed brain dysfunctions that shared many characteristics with human sepsis-associated encephalopathy. As in sepsis-associated encephalopathy, CLP-induced sickness behaviour was characterized by altered vigilance, impaired locomotor activity, sleep alteration as well as neuroendocrine and autonomic disturbances. In addition, we highlighted EEG abnormalities and rare epileptiform-like spikes in CLP mice, presenting features and proportions closed to sepsis-associated encephalopathy patients (Supplementary Fig. 3B and C). Lastly, as described in septic patients, CLP mice displayed long-term behavioural impairments. We decided to test behaviour from 15 days post-CLP, as mice presented no remaining signs of peripheral inflammation or sickness behaviour at this stage. We observed both associative and non-associative features: CLP mice displayed an enhanced anxiety during spontaneous exploration and an enhanced fear response to conditioned cues. Moreover, CLP mice presented a fear

generalization to a new auditory cue but not to a different context, a partial generalization feature that is also observed in PTSD rodent models<sup>66</sup> and in PTSD patients.<sup>67</sup> However, we observed only a limited deficit of fear extinction based on short-term spontaneous recovery, although we did not explore alternative parameters such as length of the extinction-to-test interval or reinstatement.<sup>8,68,69</sup> The *Diagnostic and Statistical Manual of Mental Disorders*, fifth edition (DSM-5) describes the key criteria to characterize PTSD in humans as the exposition to a threatening traumatic event and the persistent re-experience of this event, to which are added a range of symptoms such as avoidance, negative cognition or arousal. The sepsis-related PTSD-like syndrome described here recapitulates some key aspects of human PTSD pathology,<sup>70–72</sup> attesting to good construct and face validity. In the framework of the rodent model of PTSD,<sup>73,74</sup> CLP-induced sepsis may not constitute the acute stressor but rather acts as a pre-traumatic ‘sensitizing’ event, which promotes sustained anxiety and enhances PTSD susceptibility, the latter being assessed with a *de novo* fear conditioning at D15. In human studies, inflammation intensity is an important factor involved in PTSD susceptibility. Indeed, only 10–15% of people exposed to severe trauma will develop PTSD.<sup>75,76</sup> Both innate and environmental risk factors widely influence PTSD development susceptibility.<sup>74</sup> Among them, inflammation prior to trauma has been associated with an increased PTSD risk. A study showed that American soldiers diagnosed post-deployment with PTSD presented 2-fold higher levels of the inflammatory marker C-reactive protein before their deployment in a war zone.<sup>77</sup>

Several preclinical studies have already investigated the impact of sepsis on long-term behavioural changes.<sup>30,34,78–85</sup> Although most of them highlighted sustained anxiety, data differ mainly on aversive or non-aversive memory deficits. These divergences can

be explained by a high diversity of variables including the type and the severity of sepsis induction (liposaccharide injection or CLP), post-surgery treatments, animal species, genetic background, age and sex and, most importantly, the fear learning protocol and timing of behavioural evaluation. For instance, sepsis impaired novel object recognition at 10 days post-surgery but had no effect at 30 days.<sup>86</sup> Because many of the actual stressors in human PTSD patients are very brief,<sup>68</sup> we have favoured a short aversive pairing (only two pairings) in our fear conditioning protocol rather than a long and repetitive over-training procedure. We also avoided a longer duration stressor to prevent other confounding phenomena such as depression-like behaviour. Lastly, all the contextual or sensory cues used at D15 were unrelated to the environment where animals initially experienced sepsis (home cage), discarding any confounding re-exposure effects on behavioural measurements.

### Extended amygdala circuits mediate post-sepsis anxiety and PTSD-like fear expression

Our results showed that the pharmacological or the pharmacogenetic inhibition of the vBNST-projecting CeA neurons during the first hours following CLP suppressed long-term anxiety and PTSD-like fear expression. These data suggest that the transient activation of this circuit during acute inflammation leads to persistent modifications responsible for the long-term behavioural impairments. Those alterations may involve both cell-autonomous molecular changes—i.e. long-term reduction of extrasynaptic GABAergic receptors<sup>21</sup>—or long-term synaptic changes including afferent-specific synaptic remodelling of excitatory drive.<sup>87,88</sup> Cytokines recruited during sepsis (IL-1 $\beta$ , IL-6, TNF) have been shown to impact memory consolidation, through mechanisms ranging from long-term potentiation to synaptic scaling and neurogenesis.<sup>89</sup> Focusing on sepsis studies, CLP mice displayed long-term reduction of spine density in the BLA and the hippocampus.<sup>72,90</sup> Interestingly, the reduction of spine density in these regions has also been revealed in animal models and human patients suffering from anxiety-related disorders.<sup>91,92</sup> In our study, we have demonstrated, at a circuit scale, a causal link between the sepsis-related recruitment of the extended amygdala and the long-term PTSD-like fear expression. Given that PTSD is generally associated with hippocampal dysfunction, the hippocampus might also be involved in the post-CLP symptoms. However, in the present study, the alterations observed on contextual/cue fear memories and not on spatial/novelty tasks may indicate a preferential impact on ventral hippocampus/amygdala circuitry. Using rabies virus-based retrograde tracing, we observed that CLP induced a persistent decrease of direct inputs to vBNST-projecting CeA neurons from reticular field and BNST. Interestingly, both reticular field and BNST innervate the CeA and also receive inputs from CeA neurons, suggesting a preferred CLP-induced alteration in looped circuit elements involved in threat monitoring. The reduction of inputs onto vBNST-projecting CeA neurons suggests an unbalanced control over CeA neuronal activity, which may lead to PTSD-like exaggerated fear expression at D15 post-CLP.

This study raises the question of how peripheral infection and inflammation mediates brain activation and dysfunction. Innate immune response transduces inflammatory signals to the brain via two major pathways: the neural pathway and the humoral pathway.<sup>4</sup> Both routes might be involved in our model because the NTS (the recipient of the neural vagal inputs) and the AP (the sensor of blood-borne signals) are highly activated at 6 h post-sepsis. Local liberation of pathogen-associated molecular patterns

and cytokines during abdominal infection induces AP activation as well as peripheral nerve activation, especially the vagus nerve that projects to the NTS. The NTS/AP complex controls body temperature, blood pressure, heart rate, arousal and gut motility, all parameters highly affected during sickness behaviour in mice. The NTS/AP complex relays the signal to other autonomic and neuroendocrine hypothalamic regions, and finally cognitive/behavioural centres (via the PBN) such as the amygdala.<sup>4,93</sup> This activation cascade during the sepsis acute phase not only explains the brain activation profile at H6, but also enlightens the physiological and behavioural disturbances observed in CLP mice sickness behaviour.

### A new proactive therapeutic approach with levetiracetam prevents long-term psychocognitive impairments

The major breakthrough of this study concerns the preclinical validation of a therapeutic approach able to dampen post-infection anxiety-related syndrome using preventive administration of the neuromodulatory drug LEV only during the infection phase. Our results showed that acute LEV treatment only during the first 48 h following CLP is sufficient to alleviate long-term behavioural impairments in mice. Given that LEV application on brain slices can directly reduce synaptic transmission induced by neuronal hyperactivation while preserving baseline transmission,<sup>62</sup> and considering that we did not observe any peripheral anti-inflammatory effects of LEV (Supplementary Fig. 4B), we believe that, in our model, the action site of LEV is primarily on neuronal circuits. This drug presents all the favourable characteristics to be considered for human trials (it is well-tolerated, easy to administer and monitor and is inexpensive).<sup>38</sup> Likewise, various drugs proposed for PTSD are prescribed to sepsis survivors—including  $\beta$ -blockers,  $\alpha$ 2 adrenergic receptors agonists, corticosteroids or ketamine<sup>94</sup>—but the clinical benefit of these drugs for the prevention of post-sepsis PTSD remains highly controversial.<sup>95</sup> Surprisingly, the sepsis-induced EEG and neurophysiological changes had never been therapeutically targeted in either experimental studies or clinical trials until now, whereas a wide range of anti-epileptic drugs are available.

Using c-fos expression mapping, we showed that LEV administration had a preferential influence on brainstem activity, with a significant inhibitory effect of LEV on CLP-induced neuronal activation in the NTS and downstream regions (Fig. 5). In addition, we observed that only intraperitoneal—but not intracerebroventricular—administration of LEV could reduce CLP-induced long-term behavioural alterations, indicating that LEV may have a preferential action on the peripheral nervous system. Altogether, these data suggest that LEV could alleviate post-sepsis PTSD by acting on the vagus nerve, which senses peripheral inflammation and relays this information to the brain via the NTS. Further investigation of LEV action over the brainstem and the vagus nerve activity would be of great interest because these regions are involved in the neurovegetative response to sepsis as well as in the anti-inflammatory reflex, and are therefore directly implicated in survival.

As in most animal studies, these experiments were performed on mice in a single facility and all with the same genetic background (C57BL/6JR). The impacts of microbiota, genetic background and facility-specific factors on our findings are presently unknown. Also, sepsis can have different expression, magnitude, origin and duration, which may affect the interpretation of our



results. Given the wide associations of sepsis with a variety of neurobiological processes, including neuroinflammation and cell metabolism, it is very likely that sepsis plays additional roles to those described in our studies. In particular, other subpopulations of neurons may be affected by sepsis, as noticed by our brain-activity mapping. Additionally, the following questions remain open. What other molecular, cellular and circuit effects are triggered by sepsis and how do these effects contribute to the long-term psychocognitive outcomes? What is the exact critical period of treatment for preventing these post-sepsis outcomes? Why are some specific brain regions more susceptible to sepsis than others? Despite those important fundamental questions, the present pre-clinical findings warranted to propose, with the support of the French Ministry of Health and the TRIGGERSEP network, a multi-centre randomized clinical trial on LEV in patients with septic shock, with duration of encephalopathy and incidence of PTSD as primary and secondary outcomes (patent: US20200121644A1).

## Acknowledgements

We thank David Hardy, Patricia Reis, Flora Magno, Tarik Hissem, Carine Moigneu, Alice Dupin and Noémi Dominique for their technical support. We thank Mathilde Bigot for her input on behavioural experiments, and all the members of ‘Perception and Memory’ and ‘Experimental Neuropathology’ laboratories for their advice and comments during this work. We are grateful to Alexandru A. Hennrich and Karl-Klaus Conzelmann (Max Von Pettenkofer Institute Virology and Gene Center, Medical Faculty, Ludwig-Maximilians-University Munich, Germany) for the generous gift of (EnvA)SAD- $\Delta$ G-mCherry virus. The authors wish also to thank the Genetically Encoded Neuronal Indicator and Effector (GENIE) Project and the Janelia Farm Research Campus of the Howard Hughes Medical Institute for sharing GCaMP6f constructs, as well as the neurologic exploration group in intensive care GENER.

## Funding

The Perception and Memory laboratory receives financial support from life insurance company ‘AG2R-La-Mondiale’. The project received some financial support from the Société de Réanimation de Langue Française (SRLF), the Conseil Régional d’Île-de-France (DIM Malinf) and the Fondation pour la Recherche Médicale (FRM; #FDM201806006452).

## Competing interests

The authors report no competing interests.

## Supplementary material

[Supplementary material](#) is available at [Brain online](#).

## References

- Singer M, Deutschman CS, Seymour CW, et al. The third international consensus definitions for sepsis and septic shock (Sepsis-3). *JAMA*. 2016;315:801–810.
- Rudd KE, Johnson SC, Agesa KM, et al. Global, regional, and national sepsis incidence and mortality, 1990–2017: Analysis for the global burden of disease study. *Lancet*. 2020;395:200–211.
- Reinhart K, Daniels R, Kissoon N, Machado FR, Schachter RD, Finfer S. Recognizing sepsis as a global health priority—A WHO resolution. *N Engl J Med*. 2017;377:414–417.
- Dantzer R, O’Connor JC, Freund GG, Johnson RW, Kelley KW. From inflammation to sickness and depression: When the immune system subjugates the brain. *Nat Rev Neurosci*. 2008;9:46–56.
- Azabou E, Magalhaes E, Braconnier A, et al. Early standard electroencephalogram abnormalities predict mortality in septic intensive care unit patients. *PLoS One*. 2015;10:e0139969.
- Ely EW, Shintani A, Truman B, et al. Delirium as a predictor of mortality in mechanically ventilated patients in the intensive care unit. *JAMA*. 2004;291:1753–1762.
- Boer KR, van Ruler O, van Emmerik AAP, et al. Factors associated with posttraumatic stress symptoms in a prospective cohort of patients after abdominal sepsis: A nomogram. *Intensive Care Med*. 2008;34:664–674.
- Shalev A, Liberzon I, Marmar C. Post-traumatic stress disorder. *N Engl J Med*. 2017;376:2459–2469.
- Sharshar T, Gray F, Lorin de la Grandmaison G, et al. Apoptosis of neurons in cardiovascular autonomic centres triggered by inducible nitric oxide synthase after death from septic shock. *Lancet Lond Engl*. 2003;362:1799–1805.
- Iwashyna TJ, Ely EW, Smith DM, Langa KM. Long-term cognitive impairment and functional disability among survivors of severe sepsis. *JAMA*. 2010;304:1787–1794.
- Annane D, Sharshar T. Cognitive decline after sepsis. *Lancet Respir Med*. 2015;3:61–69.
- Schmidt K, Worrack S, Korff MV, et al. Effect of a primary care management intervention on mental health-related quality of life among survivors of sepsis. *JAMA*. 2016;315:2703–2711.
- Kapfhammer HP, Rothenhäusler HB, Krauseneck T, Stoll C, Schelling G. Posttraumatic stress disorder and health-related quality of life in long-term survivors of acute respiratory distress syndrome. *Am J Psychiatry*. 2004;161:45–52.
- Boer KR, Mahler CW, Unlu C, et al. Long-term prevalence of post-traumatic stress disorder symptoms in patients after secondary peritonitis. *Crit Care Lond Engl*. 2007;11:R30.
- Tovote P, Fadok JP, Lüthi A. Neuronal circuits for fear and anxiety. *Nat Rev Neurosci*. 2015;16:317–331.
- Adhikari A, Lerner TN, Finkelstein J, et al. Basomedial amygdala mediates top-down control of anxiety and fear. *Nature*. 2015;527:179–185.
- Fadok JP, Markovic M, Tovote P, Lüthi A. New perspectives on central amygdala function. *Curr Opin Neurobiol*. 2018;49:141–147.
- Han S, Soleiman MT, Soden ME, Zweifel LS, Palmiter RD. Elucidating an affective pain circuit that creates a threat memory. *Cell*. 2015;162:363–374.
- Yu K, Ahrens S, Zhang X, et al. The central amygdala controls learning in the lateral amygdala. *Nat Neurosci*. 2017;20:1680–1685.
- Ressler RL, Maren S. Synaptic encoding of fear memories in the amygdala. *Curr Opin Neurobiol*. 2019;54:54–59.
- Botta P, Demmou L, Kasugai Y, et al. Regulating anxiety with extrasynaptic inhibition. *Nat Neurosci*. 2015;18:1493–1500.
- Cai H, Haubensak W, Anthony TE, Anderson DJ. Central amygdala PKC- $\delta$ + neurons mediate the influence of multiple anorexigenic signals. *Nat Neurosci*. 2014;17:1240–1248.
- Tovote P, Fadok JP, Lüthi A. Neuronal circuits for fear and anxiety. *Nat Rev Neurosci*. 2015;16:317–331.

24. Adhikari A. Distributed circuits underlying anxiety. *Front Behav Neurosci.* 2014;8:112.
25. Lebow MA, Chen A. Overshadowed by the amygdala: The bed nucleus of the stria terminalis emerges as key to psychiatric disorders. *Mol Psychiatry.* 2016;21:450–463.
26. Dejager L, Pinheiro I, Dejonckheere E, Libert C. Cecal ligation and puncture: The gold standard model for polymicrobial sepsis? *Trends Microbiol.* 2011;19:198–208.
27. Rittirsch D, Huber-Lang MS, Flierl MA, Ward PA. Immunodesign of experimental sepsis by cecal ligation and puncture. *Nat Protoc.* 2009;4:31–36.
28. Pereira de Souza Goldim M, Della Giustina A, Mathias K, et al. Sickness behavior score is associated with neuroinflammation and late behavioral changes in polymicrobial sepsis animal model. *Inflammation.* 2020;43:1019–1034.
29. Osuchowski MF, Ayala A, Bahrami S, et al. Minimum quality threshold in pre-clinical sepsis studies (MQTiPSS): An international expert consensus initiative for improvement of animal modeling in sepsis. *Shock Augusta Ga.* 2018;50:377–380.
30. Calsavara AC, Rodrigues DH, Miranda AS, et al. Late anxiety-like behavior and neuroinflammation in mice subjected to sublethal polymicrobial sepsis. *Neurotox Res.* 2013;24:103–108.
31. Gao R, Li G, Yang R, Yuan H, Zhang S. Hippocampal  $\beta$ 2-microglobulin mediates sepsis-induced cognitive impairment. *Mol Med Rep.* 2018;17:7813–7820.
32. Silva AYO, Amorim ÉA, Barbosa-Silva MC, et al. Mesenchymal stromal cells protect the blood–brain barrier, reduce astrogliosis, and prevent cognitive and behavioral alterations in surviving septic mice. *Crit Care Med.* 2020;48:e290–e298.
33. Spencer-Segal JL, Singer BH, Laborc K, et al. Sepsis survivor mice exhibit a behavioral endocrine syndrome with ventral hippocampal dysfunction. *Psychoneuroendocrinology.* 2020;117:104679.
34. Singer BH, Newstead MW, Zeng X, et al. Cecal ligation and puncture results in long-term central nervous system myeloid inflammation. *PLoS One.* 2016;11:e0149136.
35. Nielsen RM, Urdanibia-Centelles O, Vedel-Larsen E, et al. Continuous EEG monitoring in a consecutive patient cohort with sepsis and delirium. *Neurocrit Care.* 2020;32:121–130.
36. Mazeraud A, Pascal Q, Verdonk F, Heming N, Chrétien F, Sharshar T. Neuroanatomy and physiology of brain dysfunction in sepsis. *Clin Chest Med.* 2016;37:333–345.
37. Sayyah M, Javad-Pour M, Ghazi-Khansari M. The bacterial endotoxin lipopolysaccharide enhances seizure susceptibility in mice: Involvement of proinflammatory factors: Nitric oxide and prostaglandins. *Neuroscience.* 2003;122:1073–1080.
38. DeWolfe JL, Szaflarski JP. Levetiracetam use in the critical care setting. *Front Neurol.* 2013;4:121.
39. Lynch BA, Lambeng N, Nocka K, et al. The synaptic vesicle protein SV2A is the binding site for the antiepileptic drug levetiracetam. *Proc Natl Acad Sci U S A.* 2004;101:9861–9866.
40. Cho JR, Koo DL, Joo EY, et al. Effect of levetiracetam monotherapy on background EEG activity and cognition in drug-naïve epilepsy patients. *Clin Neurophysiol.* 2012;123:883–891.
41. Haberman RP, Branch A, Gallagher M. Targeting neural hyperactivity as a treatment to stem progression of late-onset Alzheimer's disease. *Neurotherapeutics.* 2017;14:662–676.
42. Favrais G, Ursino M, Mouchel C, et al. Levetiracetam optimal dose-finding as first-line treatment for neonatal seizures occurring in the context of hypoxic-ischaemic encephalopathy (LEVNEONAT-1): Study protocol of a phase II trial. *BMJ Open.* 2019;9:e022739.
43. Guenther CJ, Miyamichi K, Yang HH, Heller HC, Luo L. Permanent genetic access to transiently active neurons via TRAP: Targeted recombination in active populations. *Neuron.* 2013;78:773–784.
44. Vong L, Ye C, Yang Z, Choi B, Chua S, Lowell BB. Leptin action on GABAergic neurons prevents obesity and reduces inhibitory tone to POMC neurons. *Neuron.* 2011;71:142–154.
45. Lepousez G, Alonso M, Wagner S, Gallarda BW, Lledo P-M. Selective viral transduction of adult-born olfactory neurons for chronic in vivo optogenetic stimulation. *J Vis Exp JoVE.* 2011;58:e3380.
46. Paxinos G, Franklin KJB. *The mouse brain in stereotaxic coordinates.* New York: Academic Press; 2001.
47. Walrave L, Maes K, Coppens J, et al. Validation of the 6 Hz refractory seizure mouse model for intracerebroventricularly administered compounds. *Epilepsy Res.* 2015;115:67–72.
48. Serralta A, Barcia JA, Ortiz P, Durán C, Hernández ME, Alós M. Effect of intracerebroventricular continuous infusion of valproic acid versus single i.p. and i.c.v. injections in the amygdala kindling epilepsy model. *Epilepsy Res.* 2006;70:15–26.
49. Illouz T, Madar R, Louzon Y, Griffioen KJ, Okun E. Unraveling cognitive traits using the Morris water maze unbiased strategy classification (MUST-C) algorithm. *Brain Behav Immun.* 2016;52:132–144.
50. Schwarz LA, Miyamichi K, Gao XJ, et al. Viral-genetic tracing of the input–output organization of a central noradrenergic circuit. *Nature.* 2015;524:88–92.
51. Semmler A, Hermann S, Mormann F, et al. Sepsis causes neuroinflammation and concomitant decrease of cerebral metabolism. *J Neuroinflammation.* 2008;5:38.
52. Parsons RG, Ressler KJ. Implications of memory modulation for post-traumatic stress and fear disorders. *Nat Neurosci.* 2013;16:146–153.
53. Lüthi A, Lüscher C. Pathological circuit function underlying addiction and anxiety disorders. *Nat Neurosci.* 2014;17:1635–1643.
54. Dejean C, Courtin J, Rozeske RR, et al. Neuronal circuits for fear expression and recovery: Recent advances and potential therapeutic strategies. *Biol Psychiatry.* 2015;78:298–306.
55. Lin S-C, Nicolelis MAL. Neuronal ensemble bursting in the basal forebrain encodes salience irrespective of valence. *Neuron.* 2008;59:138–149.
56. Avila I, Lin S-C. Motivational salience signal in the basal forebrain is coupled with faster and more precise decision speed. *PLoS Biol.* 2014;12:e1001811.
57. Hangya B, Ranade SP, Lorenc M, Kepecs A. Central cholinergic neurons are rapidly recruited by reinforcement feedback. *Cell.* 2015;162:1155–1168.
58. Cui Y, Lv G, Jin S, et al. A central amygdala–substantia innominata neural circuitry encodes aversive reinforcement signals. *Cell Rep.* 2017;21:1770–1782.
59. Avery SN, Clauss JA, Blackford JU. The human BNST: Functional role in anxiety and addiction. *Neuropsychopharmacology.* 2016;41:126–141.
60. Haubensak W, Kunwar PS, Cai H, et al. Genetic dissection of an amygdala microcircuit that gates conditioned fear. *Nature.* 2010;468:270–276.
61. Fukuyama K, Tanahashi S, Nakagawa M, et al. Levetiracetam inhibits neurotransmitter release associated with CICR. *Neurosci Lett.* 2012;518:69–74.
62. Meehan AL, Yang X, Yuan L-L, Rothman SM. Levetiracetam has an activity-dependent effect on inhibitory transmission. *Epilepsia.* 2012;53:469–476.
63. Stachniak TJ, Ghosh A, Sternson SM. Chemogenetic synaptic silencing of neural circuits localizes a hypothalamus→midbrain pathway for feeding behavior. *Neuron.* 2014;82:797–808.

64. Remick DG, Newcomb DE, Bolgos GL, Call DR. Comparison of the mortality and inflammatory response of two models of sepsis: Lipopolysaccharide vs. cecal ligation and puncture. *Shock Augusta Ga.* 2000;13:110–116.
65. Chinnaiyan AM, Huber-Lang M, Kumar-Sinha C, et al. Molecular signatures of sepsis. *Am J Pathol.* 2001;159:1199–1209.
66. Kaouane N, Porte Y, Vallée M, et al. Glucocorticoids can induce PTSD-like memory impairments in mice. *Science.* 2012;335:1510–1513.
67. Elzinga BM, Bremner JD. Are the neural substrates of memory the final common pathway in posttraumatic stress disorder (PTSD)? *J Affect Disord.* 2002;70:1–17.
68. Fenster RJ, Lebois LAM, Ressler KJ, Suh J. Brain circuit dysfunction in post-traumatic stress disorder: From mouse to man. *Nat Rev Neurosci.* 2018;19:535–551.
69. Kida S. Reconsolidation/destabilization, extinction and forgetting of fear memory as therapeutic targets for PTSD. *Psychopharmacology (Berl).* 2019;236:49–57.
70. Goswami S, Rodríguez-Sierra O, Cascardi M, Paré D. Animal models of post-traumatic stress disorder: Face validity. *Front Neurosci.* 2013;7:89.
71. Hendriksen H, Olivier B, Oosting RS. From non-pharmacological treatments for post-traumatic stress disorder to novel therapeutic targets. *Eur J Pharmacol.* 2014;732:139–158.
72. Huerta PT, Robbiati S, Huerta TS, et al. Preclinical models of overwhelming sepsis implicate the neural system that encodes contextual fear memory. *Mol Med.* 2016;22:789–799.
73. Deslauriers J, Toth M, Der-Avakian A, Risbrough VB. Current status of animal models of posttraumatic stress disorder: Behavioral and biological phenotypes, and future challenges in improving translation. *Biol Psychiatry.* 2018;83:895–907.
74. Bienvenu TCM, Dejean C, Jercog D, Aouizerate B, Lemoine M, Herry C. The advent of fear conditioning as an animal model of post-traumatic stress disorder: Learning from the past to shape the future of PTSD research. *Neuron.* 2021;109:2380–2397.
75. Kessler RC, Sonnega A, Bromet E, Hughes M, Nelson CB. Posttraumatic stress disorder in the national comorbidity survey. *Arch Gen Psychiatry.* 1995;52:1048–1060.
76. Kessler RC, Berglund P, Demler O, Jin R, Merikangas KR, Walters EE. Lifetime prevalence and age-of-onset distributions of DSM-IV disorders in the national comorbidity survey replication. *Arch Gen Psychiatry.* 2005;62:593.
77. Eraly SA, Nievergelt CM, Maihofer AX, et al. Assessment of plasma C-reactive protein as a biomarker of posttraumatic stress disorder risk. *JAMA Psychiatry.* 2014;71:423.
78. Savi FF, de Oliveira A, de Medeiros GF, et al. What animal models can tell us about long-term cognitive dysfunction following sepsis: A systematic review. *Neurosci Biobehav Rev.* 2021;124:386–404.
79. Gao R, Tang Y, Tong J, Yang J-J, Ji M, Zhu S. Systemic lipopolysaccharide administration-induced cognitive impairments are reversed by erythropoietin treatment in mice. *Inflammation.* 2015;38:1949–1958.
80. Yan C, Ma Z, Ma H, et al. Mitochondrial transplantation attenuates brain dysfunction in sepsis by driving microglial M2 polarization. *Mol Neurobiol.* 2020;57:3875–3890.
81. Comim CM, Freiburger V, Ventura L, et al. Inhibition of indoleamine 2,3-dioxygenase 1/2 prevented cognitive impairment and energetic metabolism changes in the hippocampus of adult rats subjected to polymicrobial sepsis. *J Neuroimmunol.* 2017;305:167–171.
82. Zhong J, Guo C, Hou W, Shen N, Miao C. Effects of MFHAS1 on cognitive impairment and dendritic pathology in the hippocampus of septic rats. *Life Sci.* 2019;235:116822.
83. Fu Q, Wu J, Zhou X-Y, et al. NLRP3/Caspase-1 pathway-induced pyroptosis mediated cognitive deficits in a mouse model of sepsis-associated encephalopathy. *Inflammation.* 2019;42:306–318.
84. Ji M-H, Qiu L-L, Tang H, et al. Sepsis-induced selective parvalbumin interneuron phenotype loss and cognitive impairments may be mediated by NADPH oxidase 2 activation in mice. *J Neuroinflammation.* 2015;12:182.
85. Gao R, Kan M, Wang S, Yang R, Zhang S. Disrupted tryptophan metabolism induced cognitive impairment in a mouse model of sepsis-associated encephalopathy. *Inflammation.* 2016;39:550–560.
86. Barichello T, Sayana P, Giridharan VV, et al. Long-term cognitive outcomes after sepsis: A translational systematic review. *Mol Neurobiol.* 2019;56:186–251.
87. Li H, Penzo MA, Taniguchi H, Kopec CD, Huang ZJ, Li B. Experience-dependent modification of a central amygdala fear circuit. *Nat Neurosci.* 2013;16:332–339.
88. Hartley ND, Gaulden AD, Báldi R, et al. Dynamic remodeling of a basolateral-to-central amygdala glutamatergic circuit across fear states. *Nat Neurosci.* 2019;22:2000–2012.
89. McAfoose J, Baune BT. Evidence for a cytokine model of cognitive function. *Neurosci Biobehav Rev.* 2009;33:355–366.
90. Chavan SS, Huerta PT, Robbiati S, et al. HMGB1 mediates cognitive impairment in sepsis survivors. *Mol Med.* 2012;18:930–937.
91. Koleske AJ. Molecular mechanisms of dendrite stability. *Nat Rev Neurosci.* 2013;14:536–550.
92. Kulkarni VA, Firestein BL. The dendritic tree and brain disorders. *Mol Cell Neurosci.* 2012;50:10–20.
93. Travaglini RA, Anselmi L. Vagal neurocircuitry and its influence on gastric motility. *Nat Rev Gastroenterol Hepatol.* 2016;13:389–401.
94. Amos T, Stein DJ, Ipser JC. Pharmacological interventions for preventing post-traumatic stress disorder (PTSD). *Cochrane Database Syst Rev.* 2014;7:CD006239.
95. Birur B, Moore NC, Davis LL. An evidence-based review of early intervention and prevention of posttraumatic stress disorder. *Community Ment Health J.* 2017;53:183–201.